# Seeking Brightness in Molecular Erbium-Based Light Upconversion

Taarit, Inès; Alves, Filipe; Benchohra, Amina; Guenee, Laure; Golesorkhi, Bahman; Rosspeintner, Arnulf; Fuerstenberg, Alexandre; Piguet, Claude

**How to cite**

TAARIT, Inès et al. Seeking Brightness in Molecular Erbium-Based Light Upconversion. In: Journal of the American Chemical Society, 2023, vol. 145, n° 15, p. 8621–8633. doi: 10.1021/jacs.3c01331

This publication URL: https://archive-ouverte.unige.ch/unige:168761
Publication DOI: 10.1021/jacs.3c01331

JACS
JOURNAL OF THE AMERICAN CHEMICAL SOCIETY
pubs.acs.org/JACS
Article

# Seeking Brightness in Molecular Erbium-Based Light Upconversion

Inès Taarit, Filipe Alves, Amina Benchohra, Laure Guénée, Bahman Golesorkhi, Arnulf Rosspeintner, Alexandre Fürstenberg, and Claude Piguet*

Cite This: J. Am. Chem. Soc. 2023, 145, 8621−8633
Read Online
ACCESS | Metrics & More | Article Recommendations | Supporting Information

**ABSTRACT:** Whereas dye-sensitized lanthanide-doped nanoparticles represent an unquestionable advance for pushing linear near-infrared (NIR) to visible-light upconversion within the frame of applications, analogous improvements are difficult to mimic for related but intramolecular processes induced at the molecular level in coordination complexes. Major difficulties arise from the cationic nature of the target cyanine-containing sensitizers (S), which drastically limits their thermodynamic affinities for catching the lanthanide activators (A) required for performing linear light upconversion. In this context, the rare previous design of stable dye-containing molecular SA light-upconverters required large S···A distances at the cost of the operation of only poorly efficient intramolecular S → A energy transfers and global sensitization. With the synthesis of the compact ligand $[\mathbf{L2}]^+$, we exploit here the benefit of using a single sulfur connector between the dye and the binding unit for counterbalancing the drastic electrostatic penalty which is expected to prevent metal complexation. Quantitative amounts of nine-coordinate $[\mathbf{L2}Er(hfac)_3]^+$ molecular adducts could be finally prepared in solution at millimolar concentrations, while the S···A distance has been reduced by 40% to reach *circa* 0.7 nm. Detailed photophysical studies demonstrate the operation of a three times improved energy transfer upconversion (ETU) mechanism for molecular $[\mathbf{L2}Er(hfac)_3]^+$ in acetonitrile at room temperature, thanks to the boosted heavy atom effect operating in the close cyanine/Er pair. NIR excitation at 801 nm can thus be upconverted into visible light (525−545 nm) with an unprecedented brightness of $B^{up}(801\ nm) = 2.0(1) \times 10^{-3}\ M^{-1}\cdot cm^{-1}$ for a molecular lanthanide complex.

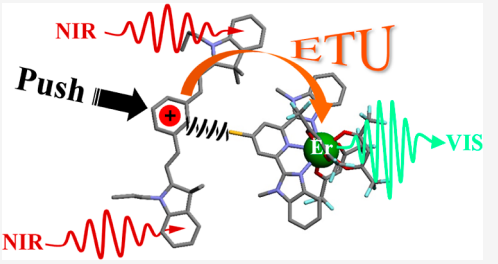


## INTRODUCTION

As soon as intense coherent laser radiation became available during the early 60s,[1−3] the predictions for inducing large anti-Stokes light upconversion processes (>100kT), relying on either the non-linear optical (NLO) response of matter[4] or the successive linear absorption of photons (upconversion),[5] could be pushed within reality.[6−12] Despite considerable efforts to chemically design sophisticated polarized chromophores for maximizing NLO responses,[13−15] the recurrent faint second-order ($\beta$) and third-order ($\gamma$) hyperpolarizability tensors limit the generation of NLO upconverted light to the use of ultra-intense excitation beams. Nowadays, the easy access to intense pulsed-femtosecond lasers ($P \approx 10^9$ W·cm$^{-2}$) opens perspectives for modern applications of NLO materials as deeply penetrating biological probes[16−19] and as optical limiting devices.[20−22] The alternative use of efficient linear absorption coefficients for the successive piling up of photons via excited-state absorption (ESA) or energy transfer upconversion (ETU) mechanisms proved to be much more efficient, and reasonable power excitation sources ($P \approx 1-10$ W·cm$^{-2}$) are compatible with the observation of upconversion processes according to the fact that long-lived real intermediate excited states are available (A* and S* in Scheme 1).[23,24] For optimizing linear light upconversion, chemists thus turned their attention toward the exploitation of long-lived intermediate excited states found as triplet levels in polyaromatic molecules[23,25−30] or as $^{2S+1}L_J$ spectroscopic levels in trivalent lanthanides doped in low-phonon ionic solids.[9−12,24,31,32] Some remarkable 15−25% upconversion quantum yields have been reported in this context.[33] Despite its attractive efficiency, the triplet−triplet annihilation (TTA) mechanism, which requires the diffusion and collision of two excited aromatic triplet acceptors, limits this methodology to intermolecular processes occurring in solution, rubbery polymeric materials, or solid matrices under anaerobic conditions since dioxygen can easily quench triplet excited states. It therefore does not fit the criteria for being considered a discrete molecular process. Consequently, miniaturization to reach nanoscopic dimensions for individual objects possessing specific light upconversion properties targeted for biological applications or solar cell technologies focused on the design and preparation of ionic nanoparticles doped with lanthanides as activators and sensitizers.

Since two decades, myriads of ESA (Scheme 1a), ETU (Scheme 1b), or related cross-relaxation and photon avalanche

Received: February 6, 2023
Published: April 5, 2023






https://doi.org/10.1021/jacs.3c01331
J. Am. Chem. Soc. 2023, 145, 8621−8633

**Scheme 1. Kinetic Diagrams Pertinent to Linear Upconversion Mechanisms Operating under Non-resonant Excitation according to (a) a Single-Center Excited-State Absorption (ESA) and (b) a Multi-Center ETU for a Sensitizer/Activator Pair[a]**

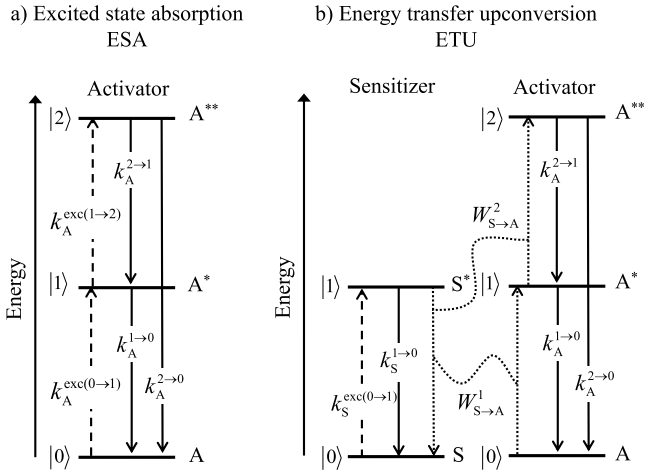


[a] $k_X^{i\to j}$ is the relaxation rate constant (radiative + non-radiative) and $k_X^{\mathrm{exc}(i\to j)}$ is the pump excitation rate constant (eq 1). $W_{S\to A}^{i}$ is the non-radiative sensitizer-to-activator energy-transfer rate constant.

mechanisms have thus been systematically investigated in these materials for pushing light upconversion into the domain of practical applications.[29−45] The increase of the surface-over-volume ratio accompanying the reduction in size from macroscopic ionic solids to nanoparticles proved to be damaging for global upconversion efficiency, but coupling to surface plasmon[46,47] or to organic dyes[48−50] overcomes this limitation by improving the linear absorption cross-sections of the sensitizers ($k_S^{\mathrm{exc}(0\to 1)}$ in Scheme 1b). However, whatever their photophysical performances, doped nanoparticles suffer from evasive reproducibility and from a lack of controlled clearance from in vivo systems. These limitations are obviously removed in molecular objects, and coordination chemists first considered to massively irradiate their preferred lanthanide complexes in order to induce light upconversion by obeying the ESA mechanism in molecules (Scheme 1a). A pioneering attempt using a tunable continuous Ti−sapphire laser NIR excitation source (780−950 nm, $P$ = 1−10 W·cm$^{-2}$) focused on solid samples of triple-helical $Na_3[Ln(2,6\text{-dipicolinate})_3]$ (Ln = Nd, Yb, and Er) only failed. This deficiency was attributed to the considerable vibrational thermal "bath" characteristic of molecular complexes, which boosts non-radiative relaxation processes ($k_A^{1\to 0}$ is very large, Scheme 1a) and limits the associated crucial lifetime of the intermediate excited level A* ($\tau_{A^*} = 1/k_A^{1\to 0}$, Scheme 1a).[51] Since the pumping rate constant $k_A^{\mathrm{exc}(m\to n)}$, modeled by eq 1,[52] is proportional to the incident pump intensity $P$ (in W·cm$^{-2}$), the use of 10 ns laser pulses with peak powers near 100 kW ($P$ > $10^9$ W·cm$^{-2}$) compensates for any short lifetimes of the intermediate excited states ($\lambda_p$ is the pump wavelength, $h$ is the Planck constant, $c$ is the speed of light in vacuum, and $\sigma_A^{m\to n}$ is the absorption cross-section of the activator-centered m → n transition (in cm$^2$), which is related to the decadic molar absorption coefficient $\varepsilon^{m\to n}$ (in M$^{-1}$·cm$^{-1}$) according to $\sigma^{m\to n} = 3.8 \times 10^{-21}\varepsilon^{m\to n}$).[53]

$$k_A^{\mathrm{exc}(m\to n)} = \frac{\lambda_p}{hc} P\sigma_A^{m\to n} = 3.8 \times 10^{-21}\frac{\lambda_p}{hc} P\varepsilon_A^{m\to n} \quad (1)$$

Consequently, ultra-intense NIR irradiation of aqueous solution of the original $Na_3[Ln(2,6\text{-dipicolinate})_3]$ (Ln = Er, Tm) complexes[54] or even of more trivial triflate salts $Tm(CF_3SO_3)_3$ in DMSO,[55] displayed faint but detectable NIR to visible-light upconversion processes. Returning to reasonable power intensities, accessible with common continuous-wave laser diodes (typically 0.1 ≤ $P$ ≤ 25 W·cm$^{-2}$), it required some efforts in chemical design for inducing detectable linear light-upconversion. The first success along those lines was reported a decade ago for an ETU mechanism implemented in a heterometallic trinuclear helicate (Figure 1a).[56] Following the report of mixed ETU/ESA mechanisms

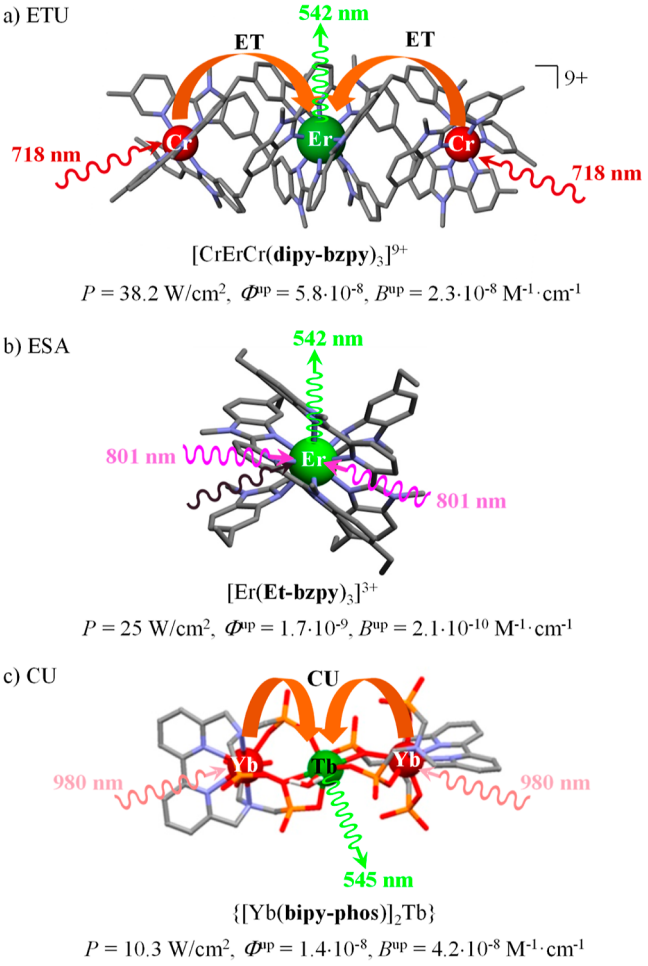


**Figure 1.** NIR to visible-light upconversion observed in dilute solution at room temperature under reasonable excitation power intensities operating in discrete (a) $[CrErCr(\mathbf{dipy\text{-}bzpy})_3]^{9+}$ (ETU, data from ref 60), (b) $[Er(\mathbf{Et\text{-}bzpy})_3]^{3+}$ (ESA, data from ref 60), and (c) $\{[Yb(\mathbf{bipy\text{-}phos})]_2Tb\}$ [cooperative upconversion (CU), data from ref 73].

operating in fluorobridged dinuclear erbium complexes,[57] a further delay was required for the reliable report of a single-center ESA mechanism detected in mononuclear triple-stranded erbium complexes under moderate NIR excitation (Figure 1b).[58,59] The overall upconversion quantum yields measured either for $[CrErCr(\mathbf{dipy\text{-}bzpy})_3]^{9+}$ (ETU, Figure 1a) or for $[Er(\mathbf{Et\text{-}bzpy})_3]^{3+}$ (ESA, Figure 1b) are similar and


https://doi.org/10.1021/jacs.3c01331
J. Am. Chem. Soc. 2023, 145, 8621−8633

amount to $\Phi_A^{up}(ESA) \simeq \Phi_{S,A}^{up}(ETU) = 1.7 \times 10^{-9}$ (normalized for $P = 25$ W·cm$^{-2}$).[60] This value remains modest as a result of combination of (i) very low intrinsic visible erbium-based quantum yields $\phi_A \approx 10^{-5}$ and (ii) short lifetimes of intermediate excited relays, A* and/or S* (see Scheme 1), that limits the upconversion efficiency factors to $\eta_A^{up}(ESA) \simeq \eta_{S,A}^{up}(ETU) \approx 10^{-4}$ in these complexes (eqn 2, $i = 0, 1$).[60]

$$\Phi^{up} = \eta^{up}\phi_A = \eta^{up}.\frac{k_{A,rad}^{2\to 0}}{\sum_i (k_{A,rad}^{2\to i} + k_{A,non\text{-}rad}^{2\to i})} \quad (2)$$

Building on this analysis, the unfavorable visible erbium molecular emitters ($\phi_{Er} \approx 10^{-5}$) have been replaced with strongly emissive terbium analogues ($\phi_{Tb} \approx 0.5$),[61] but the lack of accessible intermediate excited states that could work as relays for the successive linear piling up of photons in the $4f^8$ configuration requires two-center optical transitions,[62] in which the energy of two close sensitizers must be combined via cooperative upconversion (CU; Figure 1c).[24,63] The double-operator nature of the latter process limits its efficiency ($\eta^{up}$(CU)) by several orders of magnitude with respect to ETU or ESA mechanisms, but this drawback is balanced by the improved terbium-based intrinsic quantum yield to give the largest reported global molecular-based upconversion quantum yields $\Phi^{up} = 1.0 \times 10^{-7}$ at $P = 2.86$ W·cm$^{-2}$.[63−66] The stepwise and pioneering developments of molecular upconversion performed during the last decade have been regularly reviewed.[67−72]

Despite the systematic exploitation of highly absorbing polyaromatic sensitizers for boosting lanthanide-based down-shifting processes,[74−77] it is only recently the community has realized that the most useful parameter to assess potential applications in upconversion materials also mainly relies on the upconversion brightness $B^{up}(\lambda)$ (eq 3).[78] One can note that, for an ETU mechanism, the decadic molar absorption coefficients $\varepsilon_{abs}(\lambda)$ of the sensitizer at wavelength $\lambda$ ($\varepsilon_S^{0\to 1}$) contribute twice to the brightness via eq 3, with $\varepsilon_{abs} = \varepsilon_S^{0\to 1}$, and eq 4 ($\tau_{X,obs}^{|1\rangle}$ is the lifetime of the excited level $|1\rangle$ centered on unit X, Scheme 1b).[72]

$$B^{up}(\lambda) = \varepsilon_{abs}(\lambda)\cdot\Phi^{up}(\lambda) = \varepsilon_{abs}(\lambda)\cdot\eta^{up}\cdot\phi_A(\lambda) \quad (3)$$

$$\eta_{S,A}^{up}(ETU) \approx \left[3.8 \times 10^{-21}\left(\frac{\lambda_p}{hc}\right)\varepsilon_S^{0\to 1}P\right]W_{S\to A}^{1}W_{S\to A}^{2}(\tau_{S,obs}^{|1\rangle})^2 \tau_{A,obs}^{|1\rangle}N_A^{tot}N_S^{tot} \quad (4)$$

With this in mind, cyanine-based sensitizers relevant to the family of closed-chain cationic streptopolymethines,[79,80] which display among the largest available NIR absorption coefficients ($\varepsilon_S^{0\to 1} > 10^5$ M$^{-1}$·cm$^{-1}$),[21,48,81] have been regularly grafted onto the surface of lanthanide-doped nanoparticles for rising ETU processes.[49,82,83] Inspired by these successes, miniaturization to reach the molecular size was first attempted by Hyppänen and co-workers, who measured solution-based NIR-to-visible upconversion assigned to an ETU mechanism operating in prospective [IR-806][Er(tta)$_4$] ion pairs formed in chloroform (Figure 2a).[84] Beyond their connections to terpyridine- or phenanthroline-binding units for exploring the non-linear two-photon sensitization of [Nd(dibenzoylmethane)$_3$] in ethanol, followed by light-down-shifting (Figure 2c),[85] a cationic cyanine has been connected only once, to the best of our knowledge, to a terdentate unit

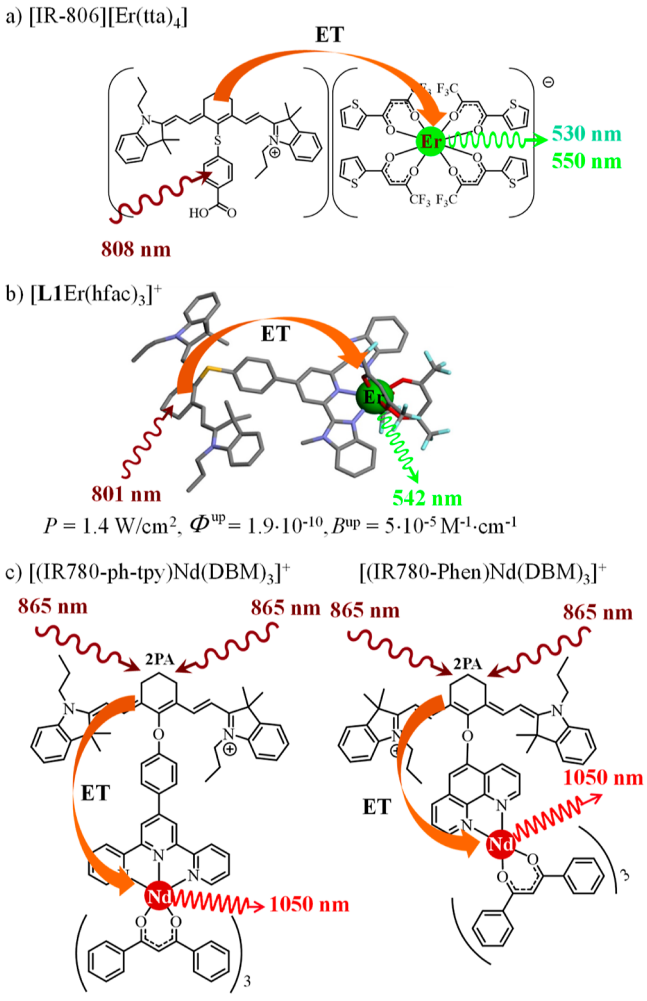


**Figure 2.** Closed-chain cationic streptopolymethines used as sensitizers for linear light upconversion via the ETU mechanism operating in solution for (a) a prospective ion pair and[84] (b) a molecular complex.[86] (c) Non-linear two-photon absorption, followed by light-downshifting operating in cyanine-containing neodymium complexes.[85]

for inducing molecular upconversion in the mononuclear [**L1**Er(hfac)$_3$]$^+$ complex according to the ETU mechanism (Figure 2b).[86] Further improvements of the upconversion quantum yields and brightness in dye-sensitized molecular complexes require (i) an increasing number of cyanine sensitizers per activator and/or (ii) a closer approach between the cyanine sensitizer and the lanthanide emitter. Both options are severely limited by the cationic nature of these cyanines, which tends to prevent the formation of stable molecular complexes with trivalent lanthanide cations.

We here propose to address the second strategy with the removal of the phenyl bridge found in ligand [**L1**]$^+$ (Figure 2b) to give the more compact terdentate receptor [**L2**]$^+$ (Scheme 2). The stability and reliable speciation of its adducts with [Ln(hfac)$_3$] in solution will be critically established prior to exploring the light upconversion process, which can then be unambiguously assigned to the molecular [**L2**Er(hfac)$_3$]$^+$ complex in solution.

## RESULTS AND DISCUSSION

### Synthesis, Molecular Structures, and Thermodynamic Stability of Ligand [L2]$^+$ and Its Lanthanide Adducts



https://doi.org/10.1021/jacs.3c01331
J. Am. Chem. Soc. 2023, 145, 8621−8633

**Scheme 2. Jablonski Diagram Established for $[L2Er(hfac)_3]^+$ Illustrating the Mechanisms for Inducing Light Upconversion through (1) Ligand-Sensitized ETU and (2) Erbium-Centered Excited-State Absorption upon 801 nm Excitation (ESA)**[a]

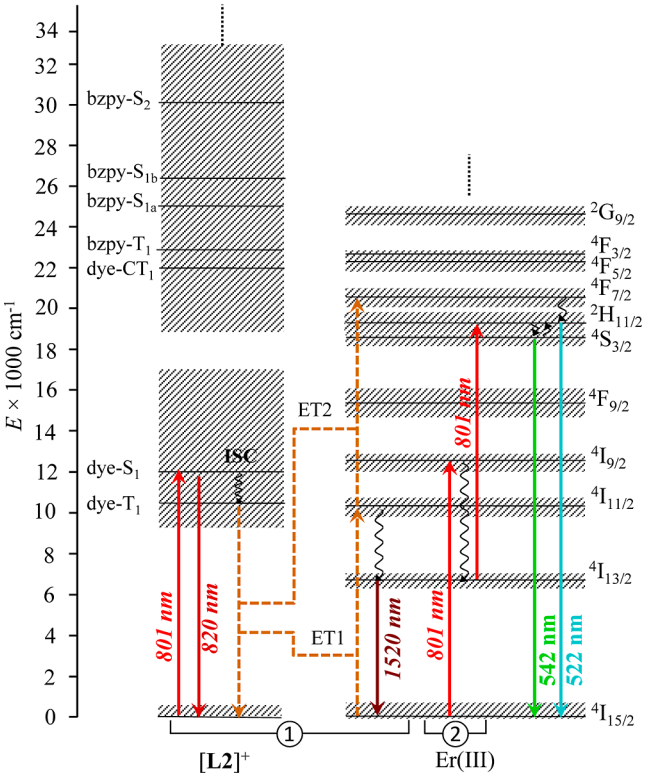


[a]ET = intramolecular S → A energy transfer; ISC = intersystem crossing. The dye-centered triplet states are located according to ref 83.

**$[L2Ln(hfac)_3]^+$ in Solution.** The cationic ligand [**L2**]I is obtained in seven steps from the starting materials **1**, **8**, **9**, and **10** (Figure 3).

Once chelidamic acid **3** was obtained,[87] two alternative synthetic strategies were considered to prepare the desired bis(methyl-benzimidazole)-bromopyridine **5**. The first one consisted in reacting **3** with *N*-methylbenzene-1,2-diamine (**10**) in $H_3PO_4$ to give the intermediate **4a** via Philips-type coupling.[88] Subsequent bromination using $PBr_5$ provided **5** in fair yield. The second strategy exploited amidation reaction with *N*-methyl-2-nitroaniline (**9**) to give the intermediate **4b**,[89] which finally provided **5** after cyclization using sodium dithionite.[90] Subsequent reaction with *S*-methylisothiourea hemisulfate yielded **6**,[91] which was deprotected with tert-butylthiolate to give **7** in good yield.[92] The ultimate nucleophilic aryl attack with the IR-780 iodide dye (**8**)[49,86] provided the desired ligand [**L2**]I with excellent yield (90%). All the NMR peaks could be successfully assigned (Figures S1−S6), and a fully satisfying high-resolution ESI-MS spectrum could be recorded (Figure S7). Finally, treatment of [**L2**]I dissolved in a minimum amount of dichloromethane with a saturated aqueous solution of $KPF_6$ quantitatively produces [**L2**]$PF_6$ after phase separation and evaporation. The removal of $I^-$ counter anions aims at limiting complications with parasitic electron exchange reactions.

The X-ray crystal structures of [**L2**]I (Tables S1−S2, Figure S8) and [**L2**]PF6 (Tables S3−S4, Figures 4a and S9) are almost superimposable. One can notice that the original red crystals give dark green solutions when dissolved in organic solvents. Care must be taken when dealing with this product, which is sensitive to light and dioxygen and should be kept in the dark under nitrogen (Figure S10). The molecular structure of the cationic ligand $[L2]^+$ shows the usual transoid−transoid arrangements of the nitrogen donor atoms, leading to a roughly coplanar terdentate benzimidazole-pyridine-benzimidazole polyaromatic binding unit (interplanar angles in the 18−33° range, Figure 4a).[93] The observed C−S−C angle of 103.9(1)° results in a close-to-orthogonal orientation of the cyanine dye with respect to the polyaromatic terdentate ligand. For comparison purposes, a similar arrangement has been reported for the cyanine segment in the extended ligand $[L1]^+$, which is connected to the phenyl bridge through a sulfur atom with a C−S−C angle of 100.3(1)°.[86] Initial attempts to crystallize the target $[L2Ln(hfac)_3]^+$ adducts by slow diffusion of diethyl ether into concentrated acetonitrile solutions in the presence of excess of triflate salts indeed provided some crystals of the biprotonated ligand $[H_2L2]^{3+}$ formed by minor and slow hydrolysis of the complex. Its crystal structure with triflate counter-anions (Tables S5−S6, Figures 4b and S11) shows that the terdentate biprotonated binding unit $[H_2L2]^{3+}$ adopts the quasi *cis*−*cis* conformation (interplanar benzimidazole-pyridine angles in the 23−27° range) stabilized by intraligand hydrogen bonding as previously found in $[H_2tpy]^{2+}$, where **tpy** stands for 2,2′;6′,2″-terpyridine.[94] The geometry of the pseudo-isosceles triangles drawn by the three nitrogen donor atoms in the two latter protonated ligands is very similar, with the central pyridine nitrogen atom occupying the apex position (Figure 4c). This leads to a flattened arrangement of the three nitrogen donor atoms compatible with the terdentate encapsulation of large guests ($d_{Ndistal-Ndistal}$ = 4.55−4.58 Å).[93] The close-to-orthogonal arrangement of the cyanine dye with respect to the terdentate ligand backbone is maintained in $[H_2L2]^{3+}$ with a C−S−C angle of 102.2°.

The thermodynamic formation of the adduct [**L2**Eu(hfac)$_3$] taken as a model for the whole lanthanide series has been studied by the NMR titration of a millimolar solution of [**L2**]$PF_6$ with the europium container [**dig**Eu(hfac)$_3$] in $CD_2Cl_2$ with an excess of diglyme ($|dig|_{tot}$ = 0.14 M; Figure S12). The $^1$H NMR spectra recorded after each addition of the lanthanide salt show the stepwise replacement of the signals of the diamagnetic free ligand $[L2]^+$ with those of the fast-relaxing paramagnetic $[L2Eu(hfac)_3]^+$ complex according to the exchange reaction summarized in eq 5. Since the concentration of diglyme is constant, equilibrium (5) is transformed into the conditional association process shown in eq 6, for which the occupancy factors $\theta_{Eu}^{L2,exp}$ and the free europium concentration of metal |Eu| = $|Eu|_{tot} - \theta_{Eu}^{L2,exp}|L2|_{tot}$ can be computed with eq 7 by simply using the integrated $^1$H NMR signals of the same proton in the free ligand $I_{L2}^H$ and in the adduct $I_{L2Eu}^H$.[95] Please note that, for the sake of clarity, |Eu| stands for |Eu(hfac)$_3$| for the rest of this work.

$$[L2]^+ + [digEu(hfac)_3] \rightleftharpoons [L2Eu(hfac)_3]^+ + dig \qquad \beta_{1,1,exch}^{L2,Eu} \qquad (5)$$



https://doi.org/10.1021/jacs.3c01331
J. Am. Chem. Soc. 2023, 145, 8621−8633

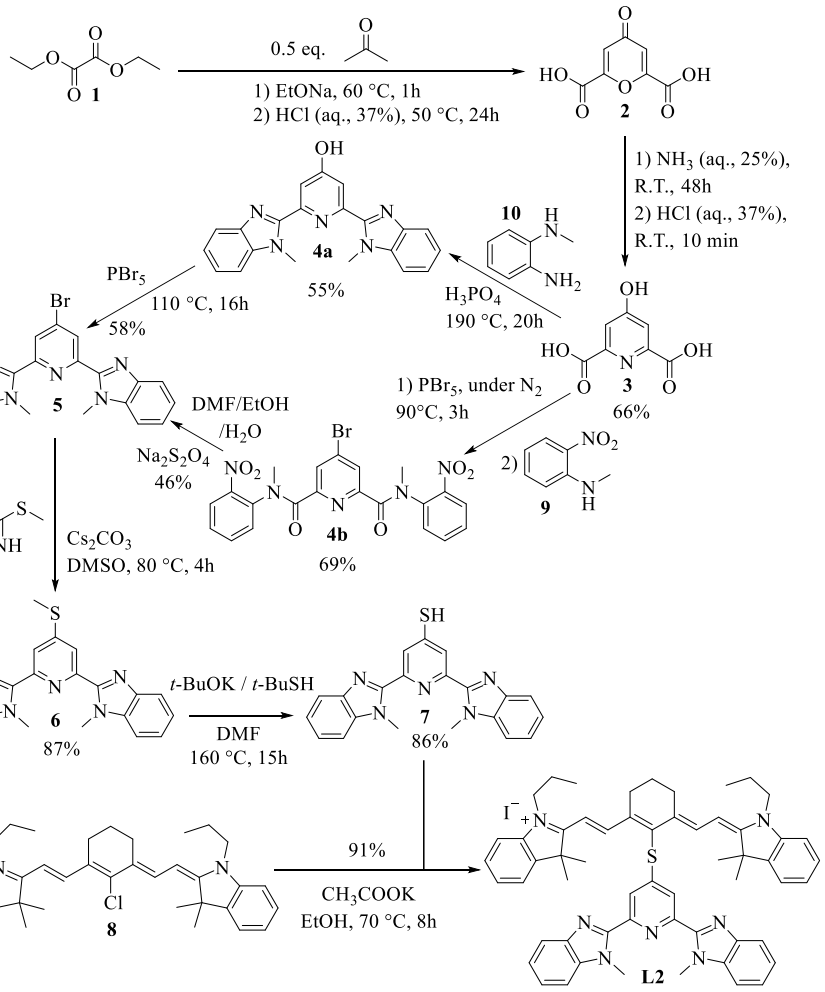


**Figure 3.** Synthesis of ligand [**L2**]I.

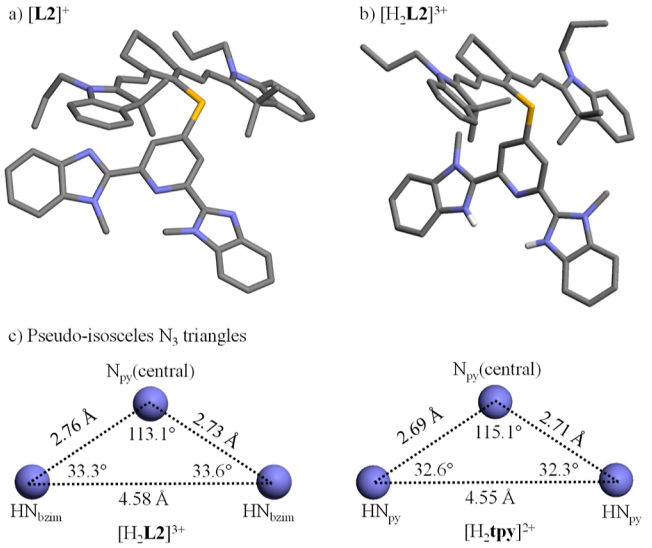


**Figure 4.** Molecular structures of the cationic ligands (a) $[\mathbf{L2}]^+$ as found in the crystal structure of $[\mathbf{L2}]PF_6$ and (b) $[H_2\mathbf{L2}]^{3+}$ observed in the crystal structure of $[H_2\mathbf{L2}](CF_3SO_3)_3$. Color code: C, gray; N, blue; S, yellow; H, white. Counter-anions and solvent molecules are omitted for clarity. (c) Geometries of the pseudo-isosceles triangles formed by the nitrogen donor atoms in the molecular structures of $[H_2\mathbf{L2}]^{3+}$ (left) and $[H_2\mathbf{tpy}]^{2+}$ (right, **tpy** = 2,2′;6′,2″-terpyridine).[94]

$$[\mathbf{L2}]^+ + [\mathrm{Eu(hfac)_3}] \rightleftharpoons [\mathbf{L2}\mathrm{Eu(hfac)_3}]^+$$
$$\beta^{\mathbf{L2},\mathrm{Eu}}_{1,1,\mathrm{asso}} = \beta^{\mathbf{L2},\mathrm{Eu}}_{1,1,\mathrm{exch}}/|\mathbf{dig}|_{\mathrm{tot}} \quad (6)$$

$$\theta^{\mathbf{L2},\mathrm{exp}}_{\mathrm{Eu}} = \frac{|\mathrm{Eu}|_{\mathrm{bound}}}{|\mathbf{L2}|_{\mathrm{tot}}} = \frac{|\mathbf{L2}\mathrm{Eu}|}{|\mathbf{L2}|_{\mathrm{tot}}} = \frac{I^{\mathrm{H}}_{\mathbf{L2}\mathrm{Eu}}}{I^{\mathrm{H}}_{\mathbf{L2}} + I^{\mathrm{H}}_{\mathbf{L2}\mathrm{Eu}}}$$
$$= \frac{|\mathrm{Eu}|_{\mathrm{tot}} - |\mathrm{Eu}|}{|\mathbf{L2}|_{\mathrm{tot}}} = \frac{\beta^{\mathbf{L2},\mathrm{Eu}}_{1,1,\mathrm{asso}} \cdot |\mathrm{Eu}|}{1 + \beta^{\mathbf{L2},\mathrm{Eu}}_{1,1,\mathrm{asso}} \cdot |\mathrm{Eu}|} \quad (7)$$

The resulting binding isotherm, i.e., $\theta^{\mathbf{L2},\mathrm{exp}}_{\mathrm{Eu}}$ plotted as a function of log(|Eu|) in Figure 5 (black diamonds), can be fitted with eq 7 to give the target conditional thermodynamic association constant $\beta^{\mathbf{L2},\mathrm{Eu}}_{1,1,\mathrm{asso}}$ = 809(74) (rebuilt red dashed trace in Figure 5), from which the exchange constant $\beta^{\mathbf{L2},\mathrm{Eu}}_{1,1,\mathrm{exch}}$ = 113(11) can be deduced with eq 6 (Table 1).

As expected from simple electrostatic considerations, the connection of the cationic dye to the terdentate binding unit reduces the affinity for catching the $[\mathbf{Ln}(\mathrm{hfac})_3]$ lanthanide container by a factor of 3 when going from the non-substituted reference ligand in $[\mathbf{L3}\mathrm{Eu}(\mathrm{hfac})_3]$ to $[\mathbf{L2}\mathrm{Eu}(\mathrm{hfac})_3]^+$ (Table 1). Surprisingly, the destabilization is even amplified for the elongated ligand $[\mathbf{L1}]^+$ since $\beta^{\mathbf{Lk},\mathrm{Y}}_{1,1,\mathrm{asso}}$ for $[\mathbf{L1}\mathrm{Y}(\mathrm{hfac})_3]^+$ is five times smaller than in $[\mathbf{L3}\mathrm{Y}(\mathrm{hfac})_3]$. One concludes that the damaging effect on the thermodynamic affinity for fixing $[\mathrm{Ln}(\mathrm{hfac})_3]$ produced by the approach of the cationic cyanine


https://doi.org/10.1021/jacs.3c01331
J. Am. Chem. Soc. 2023, 145, 8621−8633

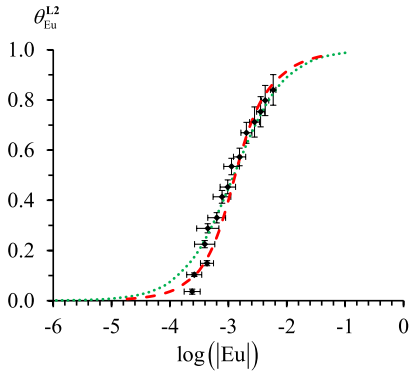


**Figure 5.** Experimental (black diamonds) and fitted (traces) binding isotherms for the titrations of ligand $[\mathbf{L2}]^+$ with $[\mathbf{dig}Eu(hfac)_3]$ in $CD_2Cl_2$ + 0.14 M diglyme at 293 K. The dashed red trace is obtained by using eq 7 and $\beta_{1,1,asso}^{L2,Eu}$ = 809(74) taken from Table 1. The dotted green trace is obtained by using eq A2-3 with $\Delta G_{1,1,asso}^{L2,Eu,\infty}$ and $\Delta G_{1,1,asso}^{L2,Eu,S}$ taken from Table A2-1 (see Appendix 2).

**Table 1. Thermodynamic Stability Constants $\beta_{1,1,asso}^{Lk,Ln}$ and $\beta_{1,1,exch}^{Lk,Ln}$ Determined for the Titrations of $[\mathbf{L1}]^+$, $[\mathbf{L2}]^+$, and L3[a] with $[\mathbf{dig}Ln(hfac)_3]$ in $CD_2Cl_2$ + 0.14 M Diglyme at 293 K**

| complex | $\beta_{1,1,asso}^{Lk,Ln}$ | $\beta_{1,1,exch}^{Lk,Ln}$ | references |
|---|---|---|---|
| $[\mathbf{L1}Y(hfac)_3]^+$ | 414(56) | 60(8) | 86 |
| $[\mathbf{L2}Eu(hfac)_3]^+$ | 809(74) | 113(11) | this work |
| $[\mathbf{L3}Eu(hfac)_3]$ | 2700(300) | 380(40) | 96 |
| $[\mathbf{L3}Y(hfac)_3]$ | 1900(400) | 270(50) | 96 |

[a]**L3** corresponds to the model terdentate ligand where the X = *S*-cyanine group attached at the 4-position of the central pyridine ring in $[\mathbf{L2}]^+$ has been removed and replaced by X = H in **L3**.

dye in going from $[\mathbf{L1}]^+$ to $[\mathbf{L2}]^+$ is more than counterbalanced by the connection of a strong sulfur donor in the 4-position of the central pyridine ring in $[\mathbf{L2}]^+$ (Figure 3).

With $\beta_{1,1,exch}^{L2,Eu}$ = 113(11) in dichloromethane (Table 1), one calculates that an equimolar mixing of $[\mathbf{L2}]^+$ and $[\mathbf{dig}Eu(hfac)_3]$ results in 91% of $[\mathbf{L2}Eu(hfac)_3]$ in solution at equilibrium, in good agreement with the associated experimental $^1$H NMR spectra recorded for a 1:1 mixture at $10^{-2}$ M (91%) and at $10^{-3}$ M (90%) (Figure S13). One, however, notices that the ratio $|\mathbf{L2}Eu(hfac)_3|/|\mathbf{L2}|$ decreases stepwise upon dilution (i.e., decomplexation becomes larger) to reach 80% at $10^{-4}$ M (Figure S13). Attempts to take into account some variable activity coefficients occurring in organic solvents, as illustrated by the dotted green trace in Figure 5 (see Appendix 2),[95] do not significantly improve the thermodynamic model and cannot rationalize the observed drift. A more convincing hypothesis assigns the latter decrease of the $|\mathbf{L2}Eu(hfac)_3|/|\mathbf{L2}|$ ratio to some competitive binding with traces of water, which are present at constant concentrations in deuterated dichloromethane to give $[(H_2O)_nEu(hfac)_3]^+$ ($n$ = 2,3). This hypothesis is corroborated by the $^1$H NMR spectra recorded for 1:1 mixtures of $[\mathbf{L2}]^+$ and diamagnetic $[\mathbf{dig}Y(hfac)_3]$ in more polar and hygroscopic deuterated acetonitrile, where a constant quantity of residual water below 20 ppm ($1.11 \times 10^{-3}$ M) is very difficult to obtain (Figure 6).[97,98] Finally, $^{19}$F NMR spectra recorded on freshly prepared solution of complexes do not show traces of trifluoroacetate anions within a period of one day.

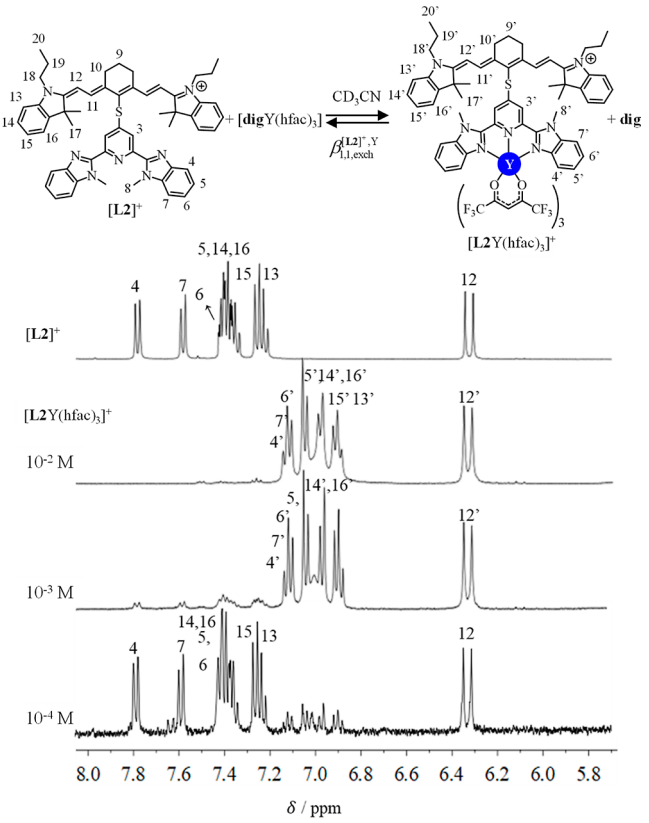


**Figure 6.** Aromatic parts of the $^1$H NMR spectra recorded for the ligand $[\mathbf{L2}]^+$ ($1 \times 10^{-2}$ M) and for its 1:1 mixture with $[\mathbf{dig}Y(hfac)_3]$ at different total concentrations in $CD_3CN$ at 293 K.

Consequently, decomplexation of the dye ligand is more pronounced and almost quantitative at $10^{-4}$ M in standard deuterated acetonitrile (Figure 6, bottom). One concludes that total concentrations equal to or larger than $10^{-4}$ M are required to ensure the quantitative formation (≥90%, Figure 6, middle) of the target adducts $[\mathbf{L2}Y(hfac)_3]^+$ and $[\mathbf{L2}Er(hfac)_3]^+$ in strictly dried acetonitrile ($CaH_2$), the solvent used for investigating the photophysical data (see next part). Finally, additional $^1$H MMR and $^{19}$F NMR titrations of $[\mathbf{L2}]^+$ in the presence of strongly paramagnetic $[\mathbf{dig}Er(hfac)_3]^+$ display broadened signals, which confirm (i) the quantitative formation of $[\mathbf{L2}Er(hfac)_3]^+$ in solution for total millimolar concentrations (Figures S14 and S15) together with (ii) the well-known partial hfac-based exchange process operating around the smallest lanthanides in these adducts (eq 8, Figure S16).[99]

$$2[\mathbf{L2}Er(hfac)_3]^+ \rightleftharpoons [\mathbf{L2}Er(hfac)_2]^{2+} + [\mathbf{L2}Er(hfac)_4] \quad (8)$$

**Molecular Structures of Lanthanide Adducts $[\mathbf{L2}Er(hfac)_3]X$ in the Solid State.** Reaction of stoichiometric amounts of $[\mathbf{L2}]PF_6$ (1.0 equiv) with $[\mathbf{dig}Er(hfac)_3]$ (1.0 equiv) in a dichloromethane/acetonitrile mixture, followed by slow diffusion of *tert*-butyl methyl ether, yielded (with difficulty) 60% of a microcrystalline powder, the elemental analysis of which is compatible with the formation of the $[\mathbf{L2}Er(hfac)_3](PF_6)$ complex (Appendix 1). The preparation of single crystals appeared to be a challenge because of the very large solubility of the complex in organic solvents, which requires the presence of competitive salts to obtain materials


https://doi.org/10.1021/jacs.3c01331
J. Am. Chem. Soc. 2023, 145, 8621−8633

suitable for X-ray diffraction studies. Systematic crystallization attempts in excess of nitrate, chloride, or triflate anions provide serendipitously small amounts of single crystals suitable for X-ray diffraction studies. The crystal structures of the complexes $[\mathbf{L2}Er(hfac)(NO_3)_2](PF_6)\cdot 2.75(C_2H_4Cl_2)$ (Tables S7 and S8, Figure S17), $[\mathbf{L2}Er(CF_3CO_2)_2Cl_2]\cdot(CH_3CH_2)_2O$ (Tables S9 and S10, Figure S18), and $[\mathbf{L2}Er(hfac)_2(CF_3CO_2)_{0.5}I_{0.5}]I\cdot C_4H_{10}O$ (Figure 7 and Tables S11 and S12, Figure S19) could

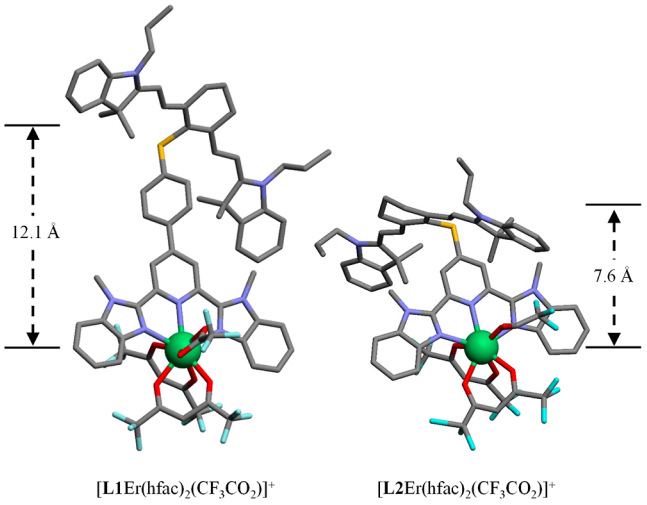


**Figure 7.** Molecular structures of $[\mathbf{L1}Er(hfac)_2(CF_3CO_2)]^+$ (left, CCDC 2091959)[86] and $[\mathbf{L2}Er(hfac)_2(CF_3CO_2)]^+$ (right)[86] as found in the crystal structures of their salts. The distances between the atom erbium and the carbon atom of the dye connected to the sulfur bridge are highlighted. Color code: C, gray; N, blue; S, yellow; O, red; F, light blue; Er, green.

be finally obtained. In all crystallized complexes, the cationic ligand $[\mathbf{L2}]^+$, as illustrated for $[\mathbf{L2}Er(hfac)_2(CF_3CO_2)]^+$ in Figure 7 (right), is meridionally tri-coordinated to the erbium metal with geometries and Er−N bond lengths analogous to those previously reported for $[\mathbf{L1}Er(hfac)_2(CF_3CO_2)]^+$ (Figure 7, left).[86] A shrinking by 40% of the average distance between the cyanine dye and the erbium activator represents the major difference in going from $[\mathbf{L1}Er(hfac)_2(CF_3CO_2)]^+$ to $[\mathbf{L2}Er(hfac)_2(CF_3CO_2)]^+$, together with a decrease of the coordination number from nine to eight (bidentate toward unidentate trifluoroacetate anion, Figure 7). Upon complexation, the C−S−C angle of the coordinated $[\mathbf{L2}]^+$ ligand remains essentially the same, as previously noticed for $[\mathbf{L1}]^+$.[86] No erbium complex containing one terdentate ligand and three $hfac^-$ anions could be crystallized with either $[\mathbf{L1}]^+$ or $[\mathbf{L2}]^+$, whereas the neutral parent ligand **L3** (free of cationic cyanine dye) provided $[\mathbf{L3}Er(hfac)_3]$ without any complication.[96] It seems reasonable to attribute these different behaviors to some improved retro-Claisen condensation of the bound $hfac^-$ co-ligand operating in the cationic adducts $[\mathbf{L}k Er(hfac)_3]^+$ ($\mathbf{L}k$ = **L1**, **L2**), which slowly provides small amounts of coordinating trifluoroacetate anions in solution.[86]

**Photophysical Properties of Ligand $[\mathbf{L2}]^+$ and Molecular Light-Upconversion Induced in Its Adduct $[\mathbf{L2}Er(hfac)_3]^+$ in Solution at Room Temperature.** The electronic absorption spectrum of $[\mathbf{L2}]^+$ recorded in acetonitrile globally mirrors that of $[\mathbf{L1}]^+$ previously reported in the same solvent (Figure 8a).[86] It is composed of two groups of bands, the first one appearing in the UV region due to electronic transitions centered on the terdentate N^N^N

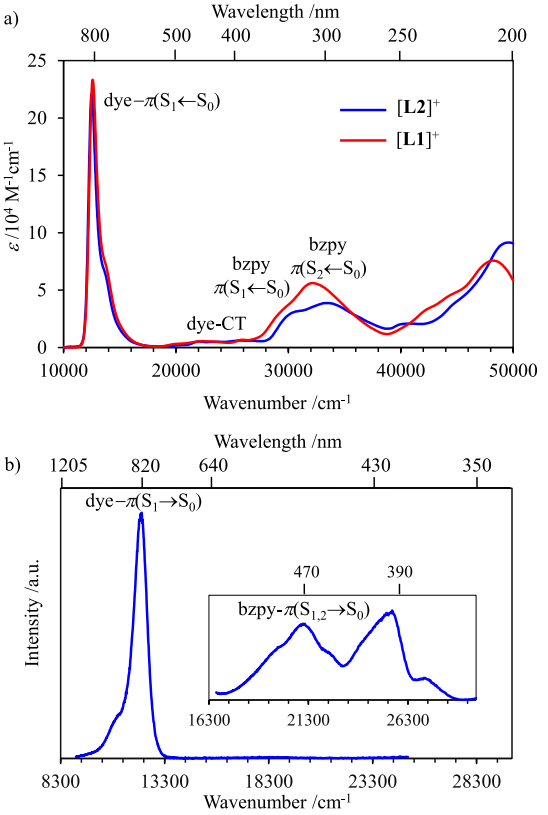


**Figure 8.** (a) Absorption spectra of the ligands $[\mathbf{L1}]^+$[86] and $[\mathbf{L2}]^+$ and (b) emission spectrum of $[\mathbf{L2}]^+$ ($\lambda_{exc}$ = 310 nm, $\tilde{\nu}_{exc}$ = 32,258 $cm^{-1}$) recorded in acetonitrile at 293 K ($10^{-6}$ M).

binding unit (bzpy; $\varepsilon^{max}_{299nm}$ = 38,750 $M^{-1}\cdot cm^{-1}$ for $[\mathbf{L2}]^+$).[100] The second group occurs in the NIR and corresponds to the intense band assigned to the cyanine part (dye, $\varepsilon^{max}_{785nm}$ = 221,000 $M^{-1}\cdot cm^{-1}$).[21,50]

We also noticed that the absorption spectra of $[\mathbf{L2}]PF_6$ or $[\mathbf{L2}]I$ are identical in solution because the counter ions do not participate in any significant intermolecular interactions. The dye then adopts the symmetrical and completely delocalized polymethine state.[101] Additionally, the absorption spectrum of $[\mathbf{L2}]^+$ roughly corresponds to the sum of those of (i) the terdentate binding unit **6** and (ii) the IR-780 iodide dye **8** taken separately (Figure S20). Due to the existence of charge-transfer (CT) bands in the cyanine part,[102] $[\mathbf{L2}]^+$ slightly absorbs in the visible domain from 22,000 to 28,000 $cm^{-1}$ with a fluctuating $\varepsilon$ = 4800−6000 $M^{-1}\cdot cm^{-1}$ (Figures 8a and S20).

Upon xenon lamp excitation at 310 nm into the bzpy($\pi^* \leftarrow \pi$) transitions centered onto the terdentate binding unit, the induced emission spectrum of $[\mathbf{L2}]^+$ is dominated by the strong dye-centered $^1\pi^* \rightarrow {}^1\pi$ transition with a maximum at 820 nm (Figure 8b), which corresponds to a 260 $cm^{-1}$ Stokes shift (Figure S21).[103] This suggests some efficient electronic communication between the terdentate binding unit and the cyanine emitter in the ligand $[\mathbf{L2}]^+$. The associated excitation spectrum recorded for $[\mathbf{L2}]^+$ ($\lambda_{analysis}$ = 800 nm) can be superimposed with its absorption spectrum (Figure S22), which corroborates the operation of an efficient electronic communication through the sulfur connector. Finally, a minor part of the ligand-based radiative relaxation detected in the visible range (inset of Figure 8b) originates from the terdentate binding site. We were, however, unable to detect delayed phosphorescence, even at 77 K in frozen solutions, in complete


https://doi.org/10.1021/jacs.3c01331
J. Am. Chem. Soc. 2023, 145, 8621−8633

agreement with the operation of negligible spin−orbit coupling and intersystem crossing processes operating in the free cyanine-containing ligand.[83] The resulting Jablonski diagram established for $[\mathbf{L2}]^+$ appears to be very similar to that previously found for $[\mathbf{L1}]^+$ (Figure S23).[86] As a last control experiment for the adequate interpretation of future linear light upconversion processes (see below), laser excitation in the dye-centered absorption band of $[\mathbf{L2}]^+$ ($\lambda_{exc}$ = 801 nm, $P$ = 7.1 W·cm$^{-2}$, acetonitrile) did not display any non-linear optical response, and no induced emission could be detected in the visible domain (Figure S24).

The mixing of stoichiometric amounts of $[\mathbf{L2}]^+$ and $[\mathbf{dig}Ln(hfac)_3]$ at millimolar concentrations in dry acetonitrile produces more than 90% of the target $[\mathbf{L2}Ln(hfac)_3]^+$ adducts (Ln = Er, Y; Figure 6). These solutions are used for the photophysical studies. The absorption spectra recorded for $[\mathbf{Lk}Er(hfac)_3]^+$ (**Lk** = **L1**, **L2**) in the visible and NIR domains (Figure 9a, 400 ≤ $\lambda$ ≤ 900 nm) are very similar and mirror

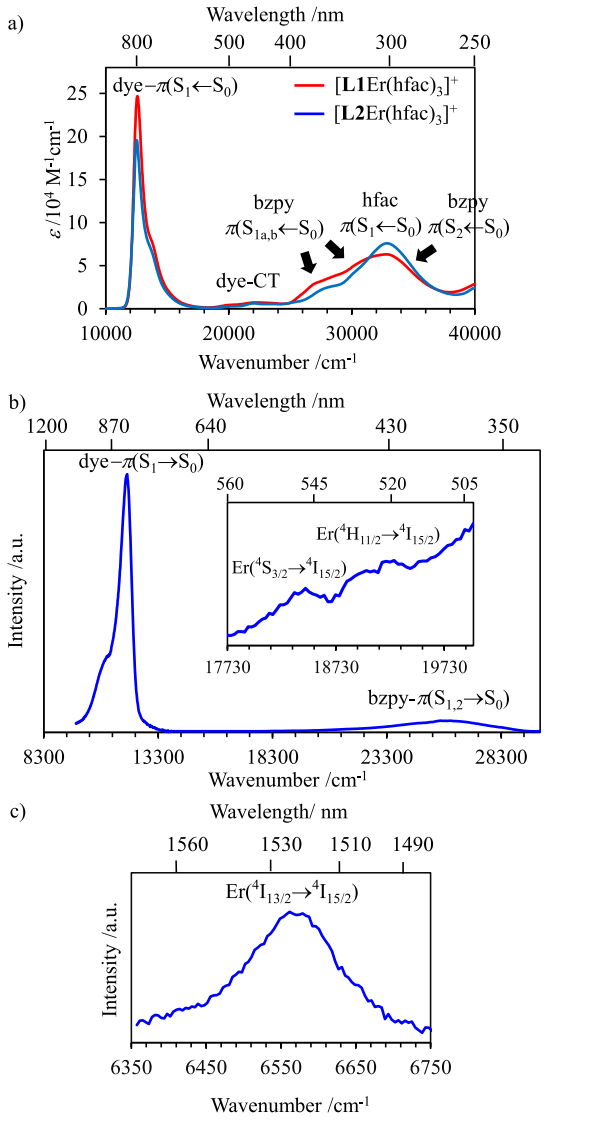


**Figure 9.** (a) Absorption spectra of the adducts $[\mathbf{L1}Er(hfac)_3]^+$[86] and $[\mathbf{L2}Er(hfac)_3]^+$ and (b,c) emission spectra of $[\mathbf{L2}Er(hfac)_3]^+$ recorded upon (b) lamp excitation ($\lambda_{exc}$ = 310 nm, $\tilde{\nu}_{exc}$ = 32,258 cm$^{-1}$) and (c) laser excitation ($\lambda_{exc}$ = 801 nm, $\tilde{\nu}_{exc}$ = 12,284 cm$^{-1}$ at $P$ = 9.9 W·cm$^{-2}$) in acetonitrile ($10^{-3}$ M, 293 K).

those recorded for the free ligands (Figure 8a) because they are dominated by the allowed electronic transitions centered on the non-perturbed cyanine parts. On the contrary, the UV domain ($\lambda$ < 400 nm) is sensitive to the complexation process since the *trans*−*trans* to *cis*−*cis* reorganization of the terdentate binding unit required for its meridional coordination to Ln(III) is accompanied by the splitting of the $\pi^* \leftarrow \pi$ transition of the lowest energy (bzpy-$\pi(S_{1a,b} \leftarrow S_0)$; Figures 9a and S25).[100] Moreover, additional $\pi^* \leftarrow \pi$ transitions, characteristic of the bound hfac$^-$ co-ligand, reinforce the absorption band around 305 nm (Figures 9a and S25). Due to the huge broad dye-centered absorption NIR band, the much weaker erbium-centered transitions occurring in the same domain ($0.01 \le \varepsilon_{Er} \le 1$ M$^{-1}$·cm$^{-1}$) cannot be distinguished.

Upon excitation on the terdentate binding unit at 310 nm ($\tilde{\nu}_{exc}$ = 32,258 cm$^{-1}$), the emission spectra of the adducts $[\mathbf{L2}Ln(hfac)_3]^+$ (Ln = Er, Figure 9b, Ln = Y, Figure S26) fairly match those of the free ligand (Figure 8b) with a strong NIR dye-centered $\pi(S_1) \rightarrow \pi(S_0)$ emission, which is slightly downshifted at $\lambda_{em}$ = 840 nm as the possible result of either partial charge localization onto the sulfur atom upon complexation in $[\mathbf{L2}Er(hfac)_3]^+$[103] or the secondary inner-filter effect due to the unavoidable millimolar concentration. An additional residual emission arises from the polyaromatic terdentate binding unit around 385 nm together with two faint, downshifted, erbium-centered visible (green) emissions (inset in Figure 9b), which could not be distinguished in the emission spectrum of $[\mathbf{L2}Y(hfac)_3]$. Their intensities are unfortunately too weak to get reliable experimental lifetimes, and the associated intrinsic quantum yields remain inaccessible. Upon subnanosecond pulsed excitation at $\lambda_{exc}$ = 375 nm, the characteristic lifetime of the latter dye-centered $\pi(S_1)$ excited state (emission at 820−840 nm) amounts to 1.26(5) ns for $[\mathbf{L2}]^+$ and reduces to 640(12) ps for $[\mathbf{L2}Er(hfac)_3]^+$ in acetonitrile at 293 K (Figure S27). This might suggest the operation of a **L2**(dye) → Er energy transfer in the complex with a global rate constant $k_{ET}^{\mathbf{L2}\rightarrow Er} = 1/\tau_{\mathbf{L2}Er} - 1/\tau_{\mathbf{L2}} = 7.7(2) \times 10^8$ s$^{-1}$ and an efficiency of $\eta_{ET}^{\mathbf{L2}\rightarrow Er} = 1 - \tau_{\mathbf{L2}Er}/\tau_{\mathbf{L2}} = 49(1)\%$. The latter interpretation corresponds to that previously proposed for rationalizing the titration of $[(IR780\text{-}Phen)]^+$ with $Nd(DBM)_3$ in acetone, where $k_{ET}^{\mathbf{Ligand}\rightarrow Nd} = 2.5 \times 10^9$ s$^{-1}$ and $\eta_{ET}^{\mathbf{Ligand}\rightarrow Nd} = 75\%$ were reported for $[(IR780\text{-}Phen)Nd(DBM)_3]^+$ (Figure 2c).[85]

However, as a control experiment, we additionally recorded the dye-centered $\pi(S_1)$ emission lifetime in $[\mathbf{L2}Y(hfac)_3]^+$, and we found that it indeed closely mirrors that found for $[\mathbf{L2}Er(hfac)_3]^+$ with $\tau_{\pi(S1)}$ = 670(13) ps (Figure S27). One concludes that the shortening of the dye-centered emission lifetime in going from $[\mathbf{L2}]^+$ to $[\mathbf{L2}Er(hfac)_3]^+$ does not reflect the operation of the sensitizer to activator energy transfer as proposed in ref 85, but it is mainly due to the heavy atom effect and spin−orbit coupling ($Z$ = 68 for erbium), which allow non-negligible intersystem crossing with $k_{ISC}^{\mathbf{L2}Er} = 1/\tau_{\mathbf{L2}Er} - 1/\tau_{\mathbf{L2}} = 7.7(2) \times 10^8$ s$^{-1}$ (efficiency $\eta_{ISC}^{\mathbf{L2}Er} = 1 - \tau_{\mathbf{L2}Er}/\tau_{\mathbf{L2}} = 49(1)\%$). Because of the smaller spin−orbit constant of yttrium ($Z$ = 39), the latter rate constant is slightly reduced and reaches $k_{ISC}^{LY} = 1/\tau_{\mathbf{L2}Y} - 1/\tau_{\mathbf{L2}} = 7.0(2) \times 10^8$ s$^{-1}$ (efficiency $\eta_{ISC}^{\mathbf{L2}Y} = 1 - \tau_{\mathbf{L2}Y}/\tau_{\mathbf{L2}} = 47(1)\%$) in $[\mathbf{L2}Y(hfac)_3]^+$. The ultimate step of indirect erbium sensitization then occurs through a ligand-to-metal energy


https://doi.org/10.1021/jacs.3c01331
J. Am. Chem. Soc. 2023, 145, 8621−8633

transfer, which implies the triplet state of the donor, in agreement with the well-accepted *antenna* mechanism proposed for lanthanide sensitization since several decades (Scheme 2).[74−76] Attempts to detect the emissions (and associated lifetimes) of the dye-centered triplet states $\pi(T_1)$ in $[\mathbf{L2}Ln(hfac)_3]^+$ (Ln = Y, Er) in the NIR domain only failed in our hands because of the negligible emission intensity arising from this level. As a support to our proposed dye → Er energy transfer mechanism, NIR excitation within the dye excitation band at $\lambda_{exc}$ = 801 nm results in a weak downshifted emission signal corresponding to the expected $Er(4I_{13/2} \rightarrow {}^4I_{15/2})$ transition (Figure 9c). One notes that the latter erbium-centered NIR emission could not be detected upon UV excitation for $[\mathbf{L2}Er(hfac)_3]^+$ ($\lambda_{exc}$ = 405 nm, Figure S28).

Alternatively, the continuous NIR diode laser excitation of $[\mathbf{L2}Er(hfac)_3]^+$ at 801 nm ($1.13 \times 10^{-3}$ M in acetonitrile at room temperature) exhibited two reasonably well-resolved upconverted emission bands detected in the visible region centered at 542 nm (18,450 $cm^{-1}$) and 522 nm (19,157 $cm^{-1}$), which can be unambiguously assigned to the erbium-centered $Er({}^4S_{3/2} \rightarrow {}^4I_{15/2})$ and $Er({}^2H_{11/2} \rightarrow {}^4I_{15/2})$ transitions, respectively (Figure 10a). No upconverted emission following

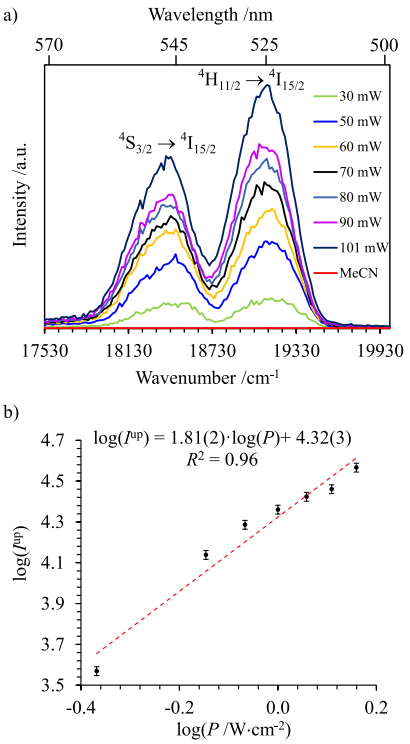


**Figure 10.** (a) Upconverted visible $Er({}^2H_{11/2} \rightarrow {}^4I_{15/2})$ and $Er({}^4S_{3/2} \rightarrow {}^4I_{15/2})$ emission bands observed for $[\mathbf{L2}Er(hfac)_3]^+$ in acetonitrile solution ($1.13 \times 10^{-3}$ M, 293 K) upon laser excitation at $\lambda_{exc}$ = 801 nm ($\tilde{\nu}_{exc}$ = 12,284 $cm^{-1}$) for variable intensity power and focused on a spot size of ∼0.07 $cm^2$. The blank corresponds to pure acetonitrile excited at 801 nm with $P$ = 5.1 W·$cm^2$. (b) Associated $\log(I^{up})-\log(P)$ plot with $P$ expressed in W·$cm^{-2}$.

801 nm NIR excitation could be recorded for solutions of either $[\mathbf{L2}Y(hfac)_3]^+$, $[\mathbf{dig}Er(hfac)_3]$, free $[\mathbf{L2}]^+$, or pure acetonitrile at room temperature (Figure S29).

Taking extreme care for (i) limiting laser exposition time for avoiding photobleaching (the solution is replaced after each measurement) and (ii) working in front face geometry for limiting absorption so that the Lambert−Beer law is obeyed for the selected incident excitation power intensities $P$ (see Appendix 3) allows the safe and unbiased record of the intensity of the upconverted $Er(4S_{3/2} \rightarrow {}^4I_{15/2})$ emission $I^{up}$ with respect to $P$ (Table S13). The associated $\log(I^{up})-\log(P)$ plot is roughly linear and returns an average slope of $n$ = 1.81(2) (Figure 10b), which confirms the successive absorption of two photons according to an ETU mechanism (Scheme 2). This value is not an integral number; this can be a consequence of many factors, such as the absorption of the upconverted emission and the involvement of nonradiative decays in populating the emissive level.[59] It can be compared with $n$ = 1.51(4) previously reported for $[\mathbf{L1}Er(hfac)_3]^+$ in similar conditions.[86] The upconversion process operating in $[\mathbf{L2}Er(hfac)_3]^+$ amounts to $\Phi^{up} = 6.0(1)\cdot10^{-10}$ at $P_{exc}$ = 1.44 W·$cm^{-2}$, which is three times larger than $\Phi^{up} = 1.9(2)\cdot10^{-10}$ ($P_{exc}$ = 1.44 W·$cm^{-2}$) reported for the extended complex $[\mathbf{L1}Er(hfac)_3]$,[+] where an additional phenyl ring separates the dye sensitizer from the erbium activator (Figure 7).[86] It is worth stressing here that the huge absorption of the dye at 801 nm is difficult to make compatible with the use of the comparative method applied here with front-face geometry for estimating the upconverting quantum yields (see Appendix 3). Since the same method was used for $[\mathbf{L1}Er(hfac)_3]^+$[85] and $[\mathbf{L2}Er(hfac)_3]^+$, comparison remains pertinent, and Table 2 collects experimental upconversion quantum yields normalized for $P$ = 25 W·$cm^{-2}$ (assuming the expected linear dependence of $\Phi^{up}$ with $P$ in the absence of the saturation phenomenon).[60,72]

Upon excitation at 801 nm, both ETU (① in Scheme 2) and ESA (② in Scheme 2) mechanisms may competitively contribute to the light upconversion operating in $[\mathbf{L2}Er(hfac)_3]^+$. Their respective modeling for molecular systems (reminiscent to Scheme 1) returns[72] the theoretical quantum yields summarized in eqs 9 and 10 ($\Phi^{up}$ = emitted photons/absorbed photons, $\lambda_p$ is the excitation wavelength at intensity $P$; $h$ and $c$ are the Planck constant and the velocity of light, respectively, $\sigma_X^{i\rightarrow j}$ is the absorption crosssection for the $i \rightarrow j$ transition on center X, $\tau_{X,obs}^{|i\rangle}$ is the observed excited lifetime of level $|i\rangle$ located on center X (X = dye or Er), $k_{Er,rad}^{2\rightarrow0}$ is the radiative lifetime, and $\phi_{Er}$ is the intrinsic quantum yield of the doubly excited erbium-centered emissive level responsible for the upconverted signal, $W_{dye\rightarrow Er}^{i}$ is the intramolecular global energy transfer rate constant, Figures S30 and S31).

$$\Phi_{Er}^{up}(ESA) \approx \left[\left(\frac{\lambda_p}{hc}\right)\sigma_{Er}^{1\rightarrow2}P\right]\tau_{Er,obs}^{|1\rangle} \times k_{Er,rad}^{2\rightarrow0}\tau_{Er,obs}^{|2\rangle} = \eta_{Er}^{up}(ESA) \times \phi_{Er} \quad (9)$$

$$\Phi_{dye,Er}^{up}(ETU) \approx \left[\left(\frac{\lambda_p}{hc}\right)\sigma_{dye}^{0\rightarrow1}P\right]W_{dye\rightarrow Er}^{1}W_{dye\rightarrow Er}^{2}(\tau_{dye,obs}^{|1\rangle})^2 \tau_{Er,obs}^{|1\rangle} \times k_{Er,rad}^{2\rightarrow0}\tau_{Er,obs}^{|2\rangle} = \eta_{dye,Er}^{up}(ETU) \times \phi_{Er} \quad (10)$$

Beyond the ratio $\sigma_{dye}^{0\rightarrow1}/\sigma_{Er}^{1\rightarrow2} \geq 250'000$, which greatly favors ETU over ESA in $[\mathbf{L2}Er(hfac)_3]^+$, the structural similitude between $[\mathbf{L2}Er(hfac)_3]^+$ and $[\mathbf{L1}Er(hfac)_3]^+$ (Figure 7) implies equivalent and negligible contribution of $\Phi_{Er}^{up}(ESA)$ to the total upconversion quantum yields in these systems.[86]


https://doi.org/10.1021/jacs.3c01331
J. Am. Chem. Soc. 2023, 145, 8621−8633

Table 2. Upconverted Quantum Yield $\Phi^{up}$ and Brightness $B^{up}$ Recorded for Molecular Complexes in Acetonitrile at Room Temperature at $P_{exc}$ = 25 W·cm$^{-2}$

| compound | $\lambda_{exc}$/nm | $\varepsilon_{max}$/M$^{-1}$·cm$^{-1}$ | $\Phi^{up}$ | $B^{up}$/M$^{-1}$·cm$^{-1}$ | mechanism[a] | reference |
|---|---|---|---|---|---|---|
| [**L2**Er(hfac)$_3$]$^+$ | 801 | 194,200 | 1.1(3) × 10$^{-8}$ | 2.0(1) × 10$^{-3}$ | ETU | this work |
| [**L1**Er(hfac)$_3$]$^+$ | 801 | 237,000 | 3.4(4) × 10$^{-9}$ | 8.0(8) × 10$^{-4}$ | ETU | 86 |
| [GaErGa(**dipy-bzpy**)$_3$]$^{9+}$ | 801 | 0.074 | 1.7(6) × 10$^{-9}$ | 1.3(5) × 10$^{-10}$ | ESA | 60 |
| [CrEr(**py-bzpy**)$_3$]$^{6+}$ | 718 | 0.10 | 3.5(3) × 10$^{-8}$ | 3.5(4) × 10$^{-9}$ | ESA + ETU | 60 |
| [CrErCr(**dipy-bzpy**)$_3$]$^{9+}$ | 718 | 0.20 | 3.8(4) × 10$^{-8}$ | 7.6(8) × 10$^{-9}$ | ESA + ETU | 60 |

[a]ESA = excited-state absorption; ETU = energy transfer upconversion.

The gain by a factor of 3 in the total upconversion quantum yield in going from [**L1**Er(hfac)$_3$]$^+$ to [**L2**Er(hfac)$_3$]$^+$ can be therefore reasonably assigned to an increase in the global energy transfer rate constants $W^i_{dye\rightarrow Er}$ (including the ISC process) contributing to $\Phi^{up}_{dye,Er}$(ETU) in the more compact complex [**L2**Er(hfac)$_3$]$^+$ (eq 10). Finally, it is worth reminding here that the useful parameter for application-oriented technologies, for instance, as light-concentrators,[33] relies on the brightness $B^{up}(\lambda)$ given in eq 3[78] and collected in Table 2 (column 5). The maximum value of $B^{up}$(801 nm) = 2.0(1) × 10$^{-3}$ M$^{-1}$·cm$^{-1}$ obtained for [**L2**Er(hfac)$_3$]$^+$ overpasses by 7 orders of magnitude the standard erbium-based ESA process measured in the triple-helical [GaErGa(**dipy-bzpy**)$_3$]$^{9+}$ complex and by almost 6 orders of magnitude that recorded in [CrErCr(**dipy-bzpy**)$_3$]$^{9+}$ where both single-center erbium-based ESA and three-center $Cr_2Er$ ETU contribute to the upconverted emission.[60]

## CONCLUSIONS

Thanks to the delicate synthesis of the oxidizable terdentate N$^\cap$N$^\cap$N binding unit 2,6-bis(1-methyl-1*H*-benzo[*d*]imidazole-2-yl)pyridine-4-thiol (**7**, Figure 3), the direct connection between the IR-780 cyanine dye (**8**) via a single sulfur atom could be realized in the cationic ligand [**L2**]$^+$. The benefit of the later design becomes obvious when one realizes that the thermodynamic affinities of [**L2**]$^+$ for [Ln(hfac)$_3$] (Ln = Eu, Y) to give the adducts [**L2**Er(hfac)$_3$]$^+$ in solution are similar to those previously reported for the extended [**L1**Er(hfac)$_3$]$^+$ complex, where the dye-lanthanide distance is larger by 40%. Consequently, close to the quantitative formation of the molecular nine-coordinate [**L2**Er(hfac)$_3$]$^+$, adducts could be obtained at millimolar concentrations where the photophysical investigations are performed. Despite the short single-atom sulfur connection between the dye and the binding unit attached to the erbium activator, the absorption and emission spectra of [**L2**Er(hfac)$_3$]$^+$ mainly reflect the characteristics of the dye and [Er(hfac)$_3$] taken separately. Compared with the free ligand [**L2**]$^+$, the connection of [Er(hfac)$_3$] in the compact [**L2**Er(hfac)$_3$]$^+$ adducts opens an efficient pathway for dye-centered singlet to triplet intersystem crossing (ISC) with $k^{L2Er}_{ISC}$ = 7.7(2) × 10$^8$ s$^{-1}$ and $\eta^{L2Er}_{ISC}$ = 49(1)% efficiency (acetonitrile, 293 K). Since dye($\pi$S1) → Er($^4I_{9/2}$) energy transfer is not efficient enough to compete significantly with the sum of ISC, radiative, and non-radiative processes affecting the excited dye($\pi$S1), the dye → Er sensitization implies dye($\pi T_1$) → Er($4I_{11/2}$) energy transfers, which are limited by efficient competition with the non-radiative relaxation of the low-energy dye($\pi T_1$) induced by some harmonics or combination bands exploiting the high-vibrational phonon bath existing in molecular complexes (Scheme 2).[51,104] Consequently, ETU results upon NIR excitation at $\lambda_{exc}$ = 801 nm to give erbium-centered green emission in [**L2**Er(hfac)$_3$]$^+$ with quantum yields and brightness, which are two to three times larger than the previous landmark settled for molecular upconversion found in [**L1**Er(hfac)$_3$]$^+$.[86] Further gain along this line would require the connection of several cyanine dyes per erbium activator, a tricky problem in terms of thermodynamic stabilities, which is currently under investigation in our laboratory.

## ASSOCIATED CONTENT

### Supporting Information

The Supporting Information is available free of charge at https://pubs.acs.org/doi/10.1021/jacs.3c01331.

Complete experimental details, ligand and complex characterizations, NMR titrations, thermodynamic analysis, and photophysical data (PDF)

### Accession Codes

CCDC 2238343, 2238348, and 223844−223847 contain the supplementary crystallographic data for this paper. These data can be obtained free of charge via www.ccdc.cam.ac.uk/data_request/cif, or by emailing data_request@ccdc.cam.ac.uk, or by contacting The Cambridge Crystallographic Data Centre, 12 Union Road, Cambridge CB2 1EZ, UK; fax: +44 1223 336033.

## AUTHOR INFORMATION


### Corresponding Author

**Claude Piguet** − *Department of Inorganic and Analytical Chemistry, University of Geneva, CH-1211 Geneva 4, Switzerland;* orcid.org/0000-0001-7064-8548; Email: Claude.Piguet@unige.ch

### Authors

**Inès Taarit** − *Department of Inorganic and Analytical Chemistry, University of Geneva, CH-1211 Geneva 4, Switzerland*

**Filipe Alves** − *Department of Inorganic and Analytical Chemistry, University of Geneva, CH-1211 Geneva 4, Switzerland;* orcid.org/0009-0004-7767-4449

**Amina Benchohra** − *Department of Inorganic and Analytical Chemistry, University of Geneva, CH-1211 Geneva 4, Switzerland*

**Laure Guénée** − *Laboratory of Crystallography, University of Geneva, CH-1211 Geneva 4, Switzerland*

**Bahman Golesorkhi** − *Department of Chemistry, University of California, Berkeley, Berkeley, California 94720, United States;* orcid.org/0000-0001-8922-3814

**Arnulf Rosspeintner** − *Department of Physical Chemistry, University of Geneva, CH-1211 Geneva 4, Switzerland;* orcid.org/0000-0002-1828-5206

**Alexandre Fürstenberg** − *Department of Inorganic and Analytical Chemistry, University of Geneva, CH-1211 Geneva 4, Switzerland;* orcid.org/0000-0002-6227-3122

Complete contact information is available at: https://pubs.acs.org/10.1021/jacs.3c01331

### Notes

The authors declare no competing financial interest.

## ■ ACKNOWLEDGMENTS

This work was supported through grants from the Swiss National Science Foundation (grants 200020_178758 and 200020_207313).

## ■ REFERENCES

(1) Maiman, T. H. Stimulated Optical Radiation in Ruby. *Nature* **1960**, *187*, 493−494.
(2) Maiman, T. H. Stimulated Optical Emission in Fluorescent Solids: 1. Theoretical Considerations. *Phys. Rev.* **1961**, *123*, 1145−1150.
(3) Maiman, T. H.; Hoskins, R. H.; D'Haenens, I. J.; Asawa, C. K.; Evtuhov, V. Stimulated Optical Emission in Fluorescent Solids. II. Spectroscopy and Stimulated Emission in Ruby. *Phys. Rev.* **1961**, *123*, 1151−1157.
(4) Goppert-Mayer, M. Elementary File with Two Quantum Fissures. *Ann. Phys.* **1931**, *9*, 273−294.
(5) Bloembergen, N. Solid State Infrared Quantum Counters. *Phys. Rev. Lett.* **1959**, *2*, 84−85.
(6) Franken, P. A.; Hill, A. E.; Peters, C. W.; Weinreich, G. Generation of Optical Harmonics. *Phys. Rev. Lett.* **1961**, *7*, 118−119.
(7) Kaiser, W.; Garrett, C. G. B. 2-Photon Excitation in $CaF_2$ - $Eu^{2+}$. *Phys. Rev. Lett.* **1961**, *7*, 229−231.
(8) Prasad, P. N.; Williams, D. J. *Introduction to Nonlinear Optical Effects in Molecules and Polymers*; John Wiley& Sons: New York-Chichester-Brisbane-Toronto-Singapore, 1991; pp 1−198.
(9) Porter, J. F. Fluorescence Excitation by the Absorption of Two Consecutive Photons. *Phys. Rev. Lett.* **1961**, *7*, 414−415.
(10) Auzel, F. Compteur Quantique par Transfert d'Energie entre deux Ions de Terres Rares dans un Tungstate Mixte et dans un Verre. *C. R. Acad. Sci.* **1966**, *B262*, 1016−1019.
(11) Auzel, F. Compteur Quantique par Transfert d'Energie de Yb(III) à Tm(III) dans un Tungstate Mixte et dans un Verre Germanate. *C. R. Acad. Sci.* **1966**, *B263*, 819−821.
(12) Auzel, F. History of Upconversion Discovery and its Evolution. *J. Lumin.* **2020**, *223*, 116900.
(13) Terenziani, F.; Katan, C.; Badaeva, E.; Tretiak, S.; Blanchard-Desce, M. Enhanced Two-Photon Absorption of Organic Chromophores: Theoretical and Experimental Assessments. *Adv. Mater.* **2008**, *20*, 4641−4678.
(14) Andraud, C.; Maury, O. Lanthanide Complexes for Nonlinear Optics: from Fundamental Aspects to Applications. *Eur. J. Inorg. Chem.* **2009**, 4357−4371.
(15) Medishetty, R.; Zareba, J. K.; Mayer, D.; Samoc, M.; Fischer, R. A. Nonlinear Optical Properties, Upconversion and Lasing in Metal-Organic Frameworks. *Chem. Soc. Rev.* **2017**, *46*, 4976−5004.
(16) Neveu, P.; Aujard, I.; Benbrahim, C.; Le Saux, T.; Allemand, J. F.; Vriz, S.; Bensimon, D.; Jullien, L. A Caged Retinoic Acid for One- and Two-Photon Excitation in Zebrafish Embryos. *Angew. Chem., Int. Ed.* **2008**, *47*, 3744−3746.
(17) Sinha, D. K.; Neveu, P.; Gagey, N.; Aujard, I.; Benbrahim-Bouzidi, C.; Le Saux, T.; Rampon, C.; Gauron, C.; Goetz, B.; Dubruille, S.; Baaden, M.; Volovitch, M.; Bensimon, D.; Vriz, S.; Jullien, L. Photocontrol of Protein Activity in Cultured Cells and Zebrafish with One- and Two-Photon Illumination. *Chembiochem* **2010**, *11*, 653−663.
(18) D'Aléo, A.; Andraud, C.; Maury, O. Two-photon Absorption of Lanthanide Complexes: from Fundamental Aspects to Biphotonic Imaging Applications. In *Luminescence of Lanthanide Ions in Coordination Compounds and Nanomaterials*; de Bettencourt-Dias, A., Ed.; Wiley: Chichester, 2014; Chapter 5, pp 197−230.
(19) Bui, A. T.; Beyler, M.; Grichine, A.; Duperray, A.; Mulatier, J.-C.; Guyot, Y.; Andraud, C.; Tripier, R.; Brasselet, S.; Maury, O. Near Infrared Two Photon Imaging Using a Bright Cationic Yb(III) Bioprobe Spontaneously Internalized Into Live Cells. *Chem. Commun.* **2017**, *53*, 6005−6008.
(20) Nguyen, T. N.; Ebrahim, F. M.; Stylianou, K. C. Photoluminescent, Upconversion Luminescent and Nonlinear Optical Metal-Organic Frameworks: From Fundamental Photophysics to Potential Applications. *Coord. Chem. Rev.* **2018**, *377*, 259−306.
(21) Pascal, S.; David, S.; Andraud, C.; Maury, O. Near-Infrared Dyes for Two-Photon Absorption in the Short-Wavelength Infrared: Strategies Towards Optical Power Limiting. *Chem. Soc. Rev.* **2021**, *50*, 6613−6658.
(22) David, S.; Chang, H. J.; Lopes, C.; Brannlund, C.; Le Guennic, B.; Berginc, G.; Van Stryland, E.; Bondar, M. V.; Hagan, D.; Jacquemin, D.; Andraud, C.; Maury, O. Benzothiadiazole-Substituted Aza-BODIPY Dyes: Two-Photon Absorption Enhancement for Improved Optical Limiting Performances in the Short-Wave IR Range. *Chem.—Eur. J.* **2021**, *27*, 3517−3525.
(23) Singh-Rachford, T. N.; Castellano, F. N. Photon Upconversion Based on Sensitized Triplet-Triplet Annihilation. *Coord. Chem. Rev.* **2010**, *254*, 2560−2573.
(24) Auzel, F. Upconversion and Anti-Stokes Processes with f and d Ions in Solids. *Chem. Rev.* **2004**, *104*, 139−174.
(25) Parker, C. A.; Hatchard, C. G. Sensitised Anti-Stokes Delayed Fluorescence. *Proc. Chem. Soc.* **1962**, 386−387.
(26) Parker, C. A.; Hatchard, C. G. Delayed Fluorescence from Solutions of Anthracene and Phenanthrene. *Proc. R. Soc. London, Ser. A* **1962**, *269*, 574−584.
(27) Parker, C. A. Sensitized P-Type Delayed Fluorescence. *Proc. R. Soc. London, Ser. A* **1963**, *276*, 125−135.
(28) Monguzzi, A.; Tubino, R.; Hoseinkhani, S.; Campione, M.; Meinardi, F. Low Power, Non-Coherent Sensitized Photon Up-Conversion: Modelling and Perspectives. *Phys. Chem. Chem. Phys.* **2012**, *14*, 4322−4332.
(29) Zhou, J.; Liu, Q.; Feng, W.; Sun, Y.; Li, F. Upconversion Luminescent Materials: Advances and Applications. *Chem. Rev.* **2015**, *115*, 395−465.
(30) Bharmoria, P.; Bildirir, H.; Moth-Poulsen, K. Triplet-Triplet Annihilation Based Near Infrared to Visible Molecular Photon Upconversion. *Chem. Soc. Rev.* **2020**, *49*, 6529−6554.
(31) Haase, M.; Schäfer, H. Upconverting Nanoparticles. *Angew. Chem., Int. Ed.* **2011**, *50*, 5808−5829.
(32) Ye, S.; Song, E.-H.; Zhang, Q.-Y. Transition Metal-Involved Photon Upconversion. *Adv. Sci.* **2016**, *3*, 1600302.
(33) Richards, B. S.; Hudry, D.; Busko, D.; Turshatov, A.; Howard, I. A. Photon Upconversion for Photovoltaics and Photocatalysis: A Critical Review. *Chem. Rev.* **2021**, *121*, 9165−9195.
(34) Chen, G.; Yang, C.; Prasad, P. N. Nanophotonics and Nanochemistry: Controlling the Excitation Dynamics for Frequency Up- and Down-conversion in Lanthanide-doped Nanoparticles. *Acc. Chem. Res.* **2013**, *46*, 1474−1486.
(35) Wang, F.; Liu, X. Multicolor Tuning of Lanthanide-doped Nanoparticles by Single Wavelength Excitation. *Acc. Chem. Res.* **2014**, *47*, 1378−1385.
(36) Yi, Z.; Luo, Z.; Qin, X.; Chen, Q.; Liu, X. Lanthanide-Activated Nanoparticles: A Toolbox for Bioimaging, Therapeutics, and Neuromodulation. *Acc. Chem. Res.* **2020**, *53*, 2692−2704.
(37) Pansare, V. J.; Hejazi, S.; Faenza, W. J.; Prud'homme, R. K. Review of Long-Wavelength Optical and NIR Imaging Materials: Contrast Agents, Fluorophores, and Multifunctional Nano Carriers. *Chem. Mater.* **2012**, *24*, 812−827.
(38) Liu, Y.; Tu, D.; Zhu, H.; Chen, X. Lanthanide-Doped Luminescent Nanoprobes: Controlled Synthesis, Optical Spectroscopy, and Bioapplications. *Chem. Soc. Rev.* **2013**, *42*, 6924−6958.

(39) Gai, S.; Li, C.; Yang, P.; Lin, J. Recent Progress in Rare Earth Micro/Nanocrystals: Soft Chemical Synthesis, Luminescent Properties, and Biomedical Applications. *Chem. Rev.* **2014**, *114*, 2343−2389.
(40) Sun, L.-D.; Wang, Y.-F.; Yan, C.-H. Paradigms and Challenges for Bioapplication of Rare Earth Upconversion Luminescent Nanoparticles: Small Size and Tunable Emission/Excitation Spectra. *Acc. Chem. Res.* **2014**, *47*, 1001−1009.
(41) Cho, U.; Chen, J. K. Lanthanide-Based Optical Probes of Biological Systems. *Cell Chem. Biol.* **2020**, *27*, 921−936.
(42) Chen, G.; Qiu, H.; Prasad, P. N.; Chen, X. Upconversion Nanoparticles: Design, Nanochemistry, and Applications in Theranostics. *Chem. Rev.* **2014**, *114*, 5161−5214.
(43) Ramasamy, P.; Manivasakan, P.; Kim, J. Y. Upconversion Nanophosphors for Solar Cell Applications. *RSC Adv.* **2014**, *4*, 34873−34895.
(44) Zhu, X.; Su, Q.; Feng, W.; Li, F. Anti-Stokes Shift Luminescent Materials for Bio-Applications. *Chem. Soc. Rev.* **2017**, *46*, 1025−1039.
(45) Zhou, J.; Leano, J. L., Jr.; Liu, Z.; Jin, D.; Wong, K.; Liu, R.; Bunzli, J. G. Impact of Lanthanide Nanomaterials on Photonic Devices and Smart Applications. *Small* **2018**, *14*, 1801882.
(46) Han, S.; Deng, R.; Xie, X.; Liu, X. Enhancing Luminescence in Lanthanide-doped Upconversion Nanoparticles. *Angew. Chem., Int. Ed.* **2014**, *53*, 11702−11715.
(47) Qin, X.; Carneiro Neto, A. N.; Longo, R. L.; Wu, Y.; Malta, O. L.; Liu, X. Surface Plasmon-Photon Coupling in Lanthanide-Doped Nanoparticles. *J. Phys. Chem. Lett.* **2021**, *12*, 1520−1541.
(48) Wang, X.-Y.; Valiev, R. R.; Ohulchanskyy, T. Y.; Agren, H.; Yang, C.; Chen, G. Dye-Sensitized Lanthanide-Doped Upconversion Nanoparticles. *Chem. Soc. Rev.* **2017**, *46*, 4150−4167.
(49) Zou, W. Q.; Visser, C.; Maduro, J. A.; Pshenichnikov, M. S.; Hummelen, J. C. Broadband Dye-Sensitized Upconversion of Near-Infrared Light. *Nat. Photonics* **2012**, *6*, 560−564.
(50) Bao, G. C.; Wen, S. H.; Lin, G. G.; Yuan, J. L.; Lin, J.; Wong, K. L.; Bunzli, J. C. G.; Jin, D. Y. Learning from Lanthanide Complexes: the Development of Dye-Lanthanide Nanoparticles and their Biomedical Applications. *Coord. Chem. Rev.* **2021**, *429*, 213642.
(51) Reinhard, C.; Güdel, H. U. High-Resolution Optical Spectroscopy of $Na_3[Ln(dpa)_3]\cdot 13H_2O$ with Ln = $Er^{3+}$, $Tm^{3+}$, $Yb^{3+}$. *Inorg. Chem.* **2002**, *41*, 1048−1055.
(52) Pollnau, M.; Gamelin, D. R.; Lüthi, S. R.; Güdel, H. U.; Hehlen, M. P. Power Dependence of Upconversion Luminescence in Lanthanide and Transition-Metal-Ion Systems. *Phys. Rev.* **2000**, *61*, 3337−3346.
(53) Schmidt, T. W.; Castellano, F. N. Photochemical Upconversion: the Primacy of Kinetics. *J. Phys. Chem. Lett.* **2014**, *5*, 4062−4072.
(54) Xiao, X.; Haushalter, J. P.; Faris, G. W. Upconversion from Aqueous Phase Lanthanide Chelates. *Opt. Lett.* **2005**, *30*, 1674−1676.
(55) Blackburn, O. A.; Tropiano, M.; Sorensen, T. J.; Thom, J.; Beeby, A.; Bushby, L. M.; Parker, D.; Natrajan, L. S.; Faulkner, S. Luminescence and Upconversion from Thulium(III) Species in Solution. *Phys. Chem. Chem. Phys.* **2012**, *14*, 13378−13384.
(56) Aboshyan-Sorgho, L.; Besnard, C.; Pattison, P.; Kittilstved, K. R.; Aebischer, A.; Bünzli, J.-C. G.; Hauser, A.; Piguet, C. Near-Infrared→Visible Light Upconversion in a Molecular Trinuclear d-f-d Complex. *Angew. Chem., Int. Ed.* **2011**, *50*, 4108−4112.
(57) Nonat, A.; Chan, C. F.; Liu, T.; Platas-Iglesias, C.; Liu, Z. Y.; Wong, W. T.; Wong, W. K.; Wong, K. L.; Charbonniere, L. J. Room Temperature Molecular Up Conversion in Solution. *Nat. Commun.* **2016**, *7*, 11978.
(58) Golesorkhi, B.; Nozary, H.; Guénée, L.; Fürstenberg, A.; Piguet, C. Room-Temperature Linear Light Upconversion in a Mononuclear Erbium Molecular Complex. *Angew. Chem., Int. Ed.* **2018**, *57*, 15172−15176.
(59) Golesorkhi, B.; Fürstenberg, A.; Nozary, H.; Piguet, C. Deciphering and Quantifying Linear Light Upconversion in Molecular Erbium Complexes. *Chem. Sci.* **2019**, *10*, 6876−6885.
(60) Golesorkhi, B.; Taarit, I.; Bolvin, H.; Nozary, H.; Jimenez, J. R.; Besnard, C.; Guenee, L.; Furstenberg, A.; Piguet, C. Molecular Light-Upconversion: We Have Had a Problem! When Excited State Absorption (ESA) Overcomes Energy Transfer Upconversion (ETU) in Cr(III)/Er(III) Complexes. *Dalton Trans.* **2021**, *50*, 7955−7968.
(61) Vanden Bussche, F.; Kaczmarek, A. M.; Van Speybroeck, V.; Van Der Voort, P.; Stevens, C. V. Overview of N-Rich Antennae Investigated in Lanthanide-Based Temperature Sensing. *Chem.—Eur. J.* **2021**, *27*, 7214−7230.
(62) Stavola, M.; Dexter, D. L. Energy transfer and two-center optical transitions involving rare-earth and OH−impurities in condensed matter. *Phys. Rev. B: Condens. Matter Mater. Phys.* **1979**, *20*, 1867−1885.
(63) Nonat, A.; Bahamyirou, S.; Lecointre, A.; Przybilla, F.; Mély, Y.; Platas-Iglesias, C.; Camerel, F.; Jeannin, O.; Charbonnière, L. J. Molecular Upconversion in Water in Heteropolynuclear Supramolecular Tb/Yb Assemblies. *J. Am. Chem. Soc.* **2019**, *141*, 1568−1576.
(64) Knighton, R. C.; Soro, L. K.; Lecointre, A.; Pilet, G.; Fateeva, A.; Pontille, L.; Frances-Soriano, L.; Hildebrandt, N.; Charbonniere, L. J. Upconversion in Molecular Hetero-Nonanuclear Lanthanide Complexes in Solution. *Chem. Commun.* **2021**, *57*, 53−56.
(65) Knighton, R. C.; Soro, L. K.; Frances-Soriano, L.; Rodriguez-Rodriguez, A.; Pilet, G.; Lenertz, M.; Platas-Iglesias, C.; Hildebrandt, N.; Charbonniere, L. J. Cooperative Luminescence and Cooperative Sensitisation Upconversion of Lanthanide Complexes in Solution. *Angew. Chem., Int. Ed.* **2022**, *61*, No. e202113114.
(66) Galico, D. A.; Murugesu, M. Controlling the Energy-Transfer Processes in a Nanosized Molecular Upconverter to Tap into Luminescence Thermometry Application. *Angew. Chem., Int. Ed.* **2022**, *61*, No. e202204839.
(67) Aboshyan-Sorgho, L.; Cantuel, M.; Petoud, S.; Hauser, A.; Piguet, C. Optical Sensitization and Upconversion in Discrete Polynuclear Chromium-Lanthanide Complexes. *Coord. Chem. Rev.* **2012**, *256*, 1644−1663.
(68) Suffren, Y.; Golesorkhi, B.; Zare, D.; Guénée, L.; Nozary, H.; Eliseeva, S. V.; Petoud, S.; Hauser, A.; Piguet, C. Taming Lanthanide-Centered Upconversion at the Molecular Level. *Inorg. Chem.* **2016**, *55*, 9964−9972.
(69) Charbonnière, L. J. Bringing Upconversion Down to the molecular Scale. *Dalton Trans.* **2018**, *47*, 8566−8570.
(70) Golesorkhi, B.; Nozary, H.; Fürstenberg, A.; Piguet, C. Erbium Complexes as Pioneers for Implementing Linear Light-Upconversion in Molecules. *Mater. Horiz.* **2020**, *7*, 1279−1296.
(71) Nonat, A. M.; Charbonnière, L. J. Upconversion of Light with Molecular and Supramolecular Lanthanide Complexes. *Coord. Chem. Rev.* **2020**, *409*, 213192.
(72) Bolvin, H.; Furstenberg, A.; Golesorkhi, B.; Nozary, H.; Taarit, I.; Piguet, C. Metal-Based Linear Light Upconversion Implemented in Molecular Complexes: Challenges and Perspectives. *Acc. Chem. Res.* **2022**, *55*, 442−456.
(73) Souri, N.; Tian, P.; Platas-Iglesias, C.; Wong, K.-L.; Nonat, A.; Charbonnière, L. J. Upconverted Photosensitization of Tb Visible Emission by NIR Yb Excitation in Discrete Supramolecular Heteropolynuclear Complexes. *J. Am. Chem. Soc.* **2017**, *139*, 1456−1459.
(74) Sabbatini, N.; Guardigli, M.; Manet, I. Antenna Effect in Encapsulation Complexes of Lanthanide Ions. *Handbook on the Physics and Chemistry of Rare Earths*; Gschneidner, K. A., Eyring, L., Eds.; Elsevier Science: Amsterdam, 1996; Vol. *23*, pp 69−120.
(75) Moore, E. G.; Samuel, A. P. S.; Raymond, K. N. From Antenna to Assay: Lessons Learned in Lanthanide Luminescence. *Acc. Chem. Res.* **2009**, *42*, 542−552.
(76) Junker, A. K. R.; Hill, L. R.; Thompson, A. L.; Faulkner, S.; Sorensen, T. J. Shining Light on the Antenna Chromophore in Lanthanide Based Dyes. *Dalton Trans.* **2018**, *47*, 4794−4803.
(77) Parker, D.; Fradgley, J. D.; Wong, K. L. The Design of Responsive Luminescent Lanthanide Probes and Sensors. *Chem. Soc. Rev.* **2021**, *50*, 8193−8213.
(78) Wong, K. L.; Bünzli, J. C. G.; Tanner, P. A. Quantum Yield and Brightness. *J. Lumin.* **2020**, *224*, 117256.


https://doi.org/10.1021/jacs.3c01331
J. Am. Chem. Soc. 2023, 145, 8621−8633

(79) Qian, G.; Wang, Z. Y. Near-Infrared Organic Compounds and Emerging Applications. *Chem.—Asian J.* **2010**, *5*, 1006−1029.
(80) Fabian, J.; Hartmann, H. *Light Absorption of Organic Colorants*; Springer: Berlin, Heidelberg, 1980; pp 162−192.
(81) Zhou, H. J.; Ren, T. B. Recent Progress of Cyanine Fluorophores for NIR-II Sensing and Imaging. *Chem.—Asian J.* **2022**, *17*, No. e202200147.
(82) Wei, W.; Chen, G.; Baev, A.; He, G. S.; Shao, W.; Damasco, J.; Prasad, P. N. Alleviating Luminescence Concentration Quenching in Upconversion Nanoparticles Through Organic Dye Sensitization. *J. Am. Chem. Soc.* **2016**, *138*, 15130−15133.
(83) Garfield, D. J.; Borys, N. J.; Hamed, S. M.; Torquato, N. A.; Tajon, C. A.; Tian, B.; Shevitski, B.; Barnard, E. S.; Suh, Y. D.; Aloni, S.; Neaton, J. B.; Chan, E. M.; Cohen, B. E.; Schuck, P. J. Enrichment of Molecular Antenna Triplets Amplifies Upconverting Nanoparticle Emission. *Nat. Photonics* **2018**, *12*, 402−407.
(84) Hyppänen, I.; Lahtinen, S.; Ääritalo, T.; Mäkelä, J.; Kankare, J.; Soukka, T. Photon Upconversion in a Molecular Lanthanide Complex in Anhydrous Solution at Room Temperature. *ACS Photonics* **2014**, *1*, 394−397.
(85) Duran-Hernandez, J.; Munoz-Rugeles, L.; Guzman-Mendez, O.; Reza, M. M.; Cadena-Caicedo, A.; Garcia-Montalvo, V.; Peon, J. Sensitization of Nd(3+) Luminescence by Simultaneous Two-Photon Excitation through a Coordinating Polymethinic Antenna. *J. Phys. Chem. A* **2022**, *126*, 2498−2510.
(86) Golesorkhi, B.; Naseri, S.; Guenee, L.; Taarit, I.; Alves, F.; Nozary, H.; Piguet, C. Ligand-Sensitized Near-Infrared to Visible Linear Light Upconversion in a Discrete Molecular Erbium Complex. *J. Am. Chem. Soc.* **2021**, *143*, 15326−15334.
(87) Terazzi, E.; Zaïm, A.; Bocquet, B.; Varin, J.; Guénée, L.; Dutronc, T.; Lemonnier, J.-F.; Floquet, S.; Cadot, E.; Heinrich, B.; Donnio, B.; Piguet, C. Implementing Liquid-Crystalline Properties in Single-Stranded Dinuclear Lanthanide Helicates. *Eur. J. Inorg. Chem.* **2013**, 3323−3333.
(88) Addison, A. W.; Rao, T. N.; Wahlgren, C. G. Synthesis of Some Benzimidazole- and Benzothiazole-Derived Ligand Systems and their Precursory Diacids. *J. Heterocycl. Chem.* **1983**, *20*, 1481−1484.
(89) Piguet, C.; Bocquet, B.; Hopfgartner, G. Syntheses of Segmental Heteroleptic Ligands for the Self-Assembly of Heteronuclear Helical Supramolecular Complexes. *Helv. Chim. Acta* **1994**, *77*, 931−942.
(90) McKenzie, B. M.; Miller, A. K.; Wojtecki, R. J.; Johnson, J. C.; Burke, K. A.; Tzeng, K. A.; Mather, P. T.; Rowan, S. J. Improved synthesis of functionalized mesogenic 2,6-bisbenzimidazolylpyridine ligands. *Tetrahedron* **2008**, *64*, 8488−8495.
(91) Zhang, C. Y.; Zhou, Y.; Huang, J. T.; Tu, C. H.; Zhou, X. A.; Yin, G. D. Cesium Carbonate-Promoted Synthesis of Aryl Methyl Sulfides Using S-Methylisothiourea Sulfate Under Transition-Metal-Free Conditions. *Org. Biomol. Chem.* **2018**, *16*, 6316−6321.
(92) Pinchart, A.; Dallaire, C.; Van Bierbeek, A.; Gingras, M. Efficient Formation of Aromatic Thiols from Thiomethylated Precursors. *Tetrahedron Lett.* **1999**, *40*, 5479−5482.
(93) Hoang, T. N. Y.; Lathion, T.; Guénée, L.; Terazzi, E.; Piguet, C. Protonation and Complexation Properties of Polyaromatic Terdentate Six-Membered Chelate Ligands. *Inorg. Chem.* **2012**, *51*, 8567−8575.
(94) Berthon, C.; Grigoriev, M. S. 2,2′:6′,2″-Terpyridinium Dinitrate. *Acta Crystallogr., Sect. E: Struct. Rep. Online* **2005**, *61*, O1216−O1217.
(95) Baudet, K.; Kale, V.; Mirzakhani, M.; Babel, L.; Naseri, S.; Besnard, C.; Nozary, H.; Piguet, C. Neutral Heteroleptic Lanthanide Complexes for Unravelling Host-Guest Assemblies in Organic Solvents: The Law of Mass Action Revisited. *Inorg. Chem.* **2020**, *59*, 62−75.
(96) Naseri, S.; Mirzakhani, M.; Besnard, C.; Guenee, L.; Briant, L.; Nozary, H.; Piguet, C. Preorganized Polyaromatic Soft Terdentate Hosts for the Capture of [Ln(beta-diketonate)(3)] Guests in Solution. *Chem.—Eur. J.* **2023**, *29*, No. e202202727.
(97) Takamuku, T.; Tabata, M.; Yamaguchi, A.; Nishimoto, J.; Kumamoto, M.; Wakita, H.; Yamaguchi, T. Liquid Structure of Acetonitrile-Water Mixtures by X-ray Diffraction and Infrared Spectroscopy. *J. Phys. Chem. B* **1998**, *102*, 8880−8888.
(98) Ewing, M. B.; Ochoa, J. C. S. Vapor Pressures of Acetonitrile Determined by Comparative Ebulliometry. *J. Chem. Eng. Data* **2004**, *49*, 486−491.
(99) Zaïm, A.; Favera, N. D.; Guénée, L.; Nozary, H.; Hoang, T. N. Y.; Eliseeva, S. V.; Petoud, S.; Piguet, C. Lanthanide hexafluoroacetylacetonates vs. nitrates for the controlled loading of luminescent polynuclear single-stranded oligomers. *Chem. Sci.* **2013**, *4*, 1125−1136.
(100) Piguet, C.; Bünzli, J.-C. G.; Bernardinelli, G.; Bochet, C. G.; Froidevaux, P. Design of Luminescent Building Blocks for Supramolecular Triple-Helical Lanthanide Complexes. *J. Chem. Soc., Dalton Trans.* **1995**, 83−97.
(101) Pascal, S.; Chi, S. H.; Perry, J. W.; Andraud, C.; Maury, O. Impact of Ion-Pairing Effects on Linear and Nonlinear Photophysical Properties of Polymethine Dyes. *Chemphyschem* **2020**, *21*, 2536−2542.
(102) Jarman, J. B.; Dougherty, D. A. Charge- Transfer Heptamethine Dyes for NIR Singlet Oxygen Generation. *Chem. Commun.* **2019**, *55*, 5511−5514.
(103) Sissa, C.; Painelli, A.; Terenziani, F.; Trotta, M.; Ragni, R. About the Origin of the Large Stokes Shift in Aminoalkyl Substituted Heptamethine Cyanine Dyes. *Phys. Chem. Chem. Phys.* **2020**, *22*, 129−135.
(104) Coelho, J. A. A.; Moura, R. T.; Longo, R. L.; Malta, O. L.; Carneiro Neto, A. N. Modeling the Eu(III)-to-Cr(III) Energy Transfer Rates in Luminescent Bimetallic Complexes. *Inorganics* **2023**, *11*, 38.




https://doi.org/10.1021/jacs.3c01331
J. Am. Chem. Soc. 2023, 145, 8621−8633